

THE DETERIORATION IN HEAT TRANSFER  
TO FLUIDS AT SUPER-CRITICAL PRESSURE  
AND HIGH HEAT FLUXES

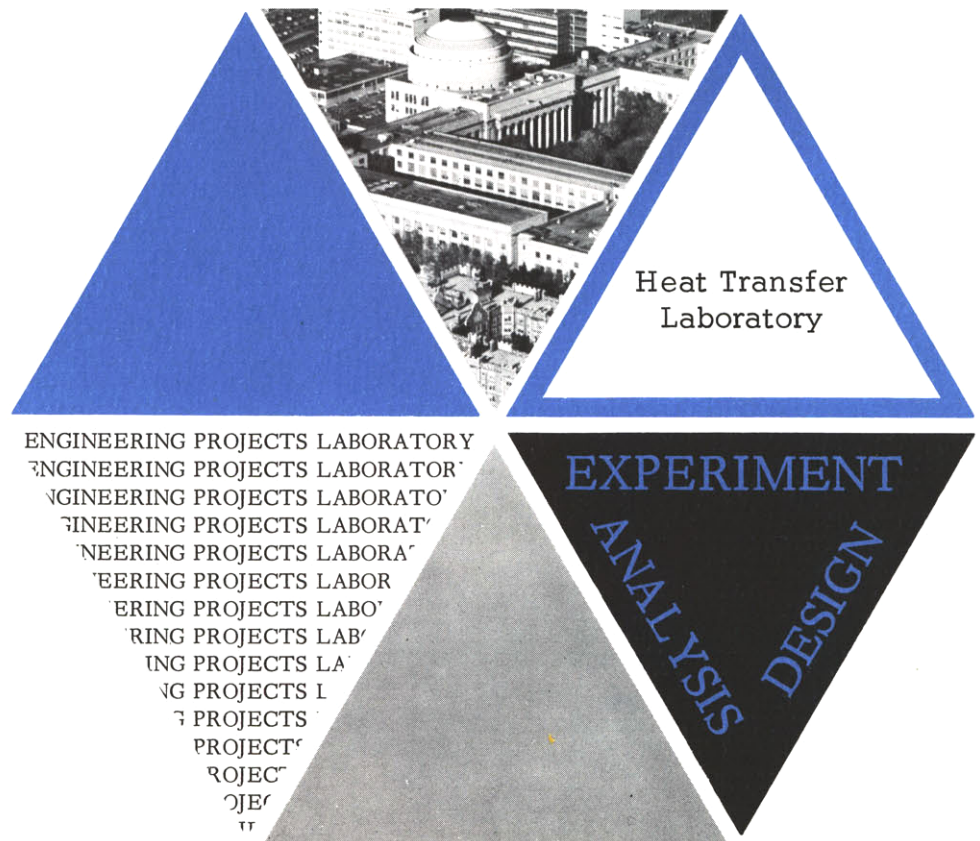
Bharat S. Shiralkar

Peter Griffith

Report No. 70332-51

Department of Mechanical  
Engineering  
Engineering Projects Laboratory  
Massachusetts Institute of  
Technology

March 1, 1968



THE DETERIORATION IN HEAT TRANSFER TO FLUIDS AT  
SUPER-CRITICAL PRESSURE AND HIGH HEAT FLUXES

by

Bharat S. Shiralkar

Peter Griffith

Sponsored by

American Electric Power Service Corp.

March 1, 1968

Engineering Projects Laboratory  
Department of Mechanical Engineering  
Massachusetts Institute of Technology  
Cambridge, Massachusetts

02139

## TABLE OF CONTENTS

1.	INTRODUCTION	1
2.	SCOPE OF PRESENT INVESTIGATION	3
3.	EXPERIMENTAL EVIDENCE OF PREVIOUS INVESTIGATORS	4
4.	PROPERTIES AND THERMODYNAMICS NEAR THE CRITICAL POINT	7
5.	THEORETICAL APPROACH	9
	1. Introduction	9
	2. Basic Equations	9
	3. Expressions for the Eddy Diffusivity	16
	4. Method of Solution	20
	5. Results	21
	6. Simplified Physical Model	27
	7. Safe Versus Unsafe Plot for Steam	35
6.	EXPERIMENTAL APPROACH	37
	1. Introduction	37
	2. Description of Apparatus	37
	3. Capabilities and Measurements	39
	4. Experimental Results	40
	5. Factors Affecting Deterioration	43
	6. Comparison with Computed Wall Temperature Versus Bulk Enthalpy	46
	7. Experimental Safe Versus Unsafe Plot for CO <sub>2</sub>	46
	8. Comparison Between Upflow and Downflow	49
7.	FUTURE WORK	55
8.	CONCLUSIONS	56
9.	REFERENCES	57

## LIST OF FIGURES

Fig.		Page
1.	Variation of the Heat Transfer Coefficient with Heat Flux in the Critical Region (From Ref. 33)	2
2.	Deteriorated Heat Transfer Region (Shitsman)	5
3.	State Diagram for Steam	8
4.	Properties of Water in Critical Region (From Swenson and Kakagrla)	8
5.	Coordinate System for Flow of Fluid	10
6.	Computed Results: Mass Flow Rate Versus Bulk Enthalpy for System	22
7.	Computed Results: Mass Flow Rate Versus Bulk Enthalpy for System	23
8.	Computed Results: Mass Flow Rate Versus Bulk Enthalpy for System	24
9.	Computed Results: Mass Flow Rate Versus Bulk Enthalpy for System	25
10.	Deteriorated Heat Transfer Region (Shitsman)	26
11.	Computed Results: Constant Shear Stress Lines	28
12.	Variation of Shear Stress with Heat Flux	29
13.	Computed Velocity Profiles	30
14.	Computed Temperature Profiles	31
15.	Radial Locus of $T_c$ in a Typically Deteriorated Region	32
16.	Physical Explanation of Heat Transfer Variation	34
17.	Computed Safe Versus Unsafe Plot for System	36
18.	Schematic Drawing of Experimental Loop	38
19.	Data Print-Out	41
20.	Experimental Results for $CO_2$ at 1100 Psi	42
21.	Experimental Results Showing Effect of Inlet Enthalpy on the Temperature Versus Length Profile	44
22.	Experimental Results Showing Effect of Tube Vibration	45
23.	Experimental Results for CO at 1150 Psi	47
24.	Comparison Between Computed and Experimental Wall Temperature Profiles for $CO_2$	48

LIST OF FIGURES (Continued)

Fig.		Page
25.	Experimental Safe Versus Unsafe Plot for CO <sub>2</sub> at 1100 Psi	50
26.	Experimental Safe Versus Unsafe Plot for CO <sub>2</sub> at 1150 Psi	51
27.	Comparison Between Computed and Experimental Safe Versus Unsafe Plots	52
28.	Experimental Results for Downflow	53
29.	Experimental Safe Versus Unsafe Plot for Downflow	54

## NOMENCLATURE

C <sub>p</sub>	local specific heat at constant pressure, ( BTU/lb <sup>o</sup> F)
C <sub>p<sub>o</sub></sub>	reference value of specific heat, ( BTU/lb <sup>o</sup> F)
D	diameter of tube, (ft.)
g	acceleration due to gravity, (ft/hr. <sup>2</sup> )
G	mass flow rate, (lbs/ft <sup>2</sup> -hr.)
Gr	Grashof Number = $(\rho_b - \rho_o)/\rho_o \times (\rho_o/\mu_o)^2 \gamma^3 g$
h'	heat transfer coefficient, (BTU/ft <sup>2</sup> - <sup>o</sup> F-hr)
h	local enthalpy, (BTU/lbs.)
H	bulk mean enthalpy at a cross-section (BTU/lb)
k	local conductivity, (BTU/ft-hr- <sup>o</sup> F)
k <sub>o</sub>	reference value of thermal conductivity, (BTU/ft-hr- <sup>o</sup> F)
K	constant = 0.36
L	length along tube, (ft.)
n	constant = 0.124
Nu	Nusselt Number = hD/k
Nu <sub>mac</sub>	MacAdams' Nusselt Number = $0.023(Re_b)^{0.8}(Pr)^{0.4}$
p	pressure, (lbs/ft. <sup>2</sup> )
Pr	Prandtl Number = $C_p\mu/k$
P <sub>ro</sub>	$C_p\mu_o/k_o$
q	local heat flux, (BTU/ft <sup>2</sup> -hr)
Q <sub>o</sub> /A	wall heat flux (BTU/ft <sup>2</sup> -hr)
R	radius of tube, (ft)
Re	Reynolds Number = $GD/\mu$
T	temperature ( <sup>o</sup> F)
U	local velocity, axial, (ft/hr)
U <sup>+</sup>	$U/\sqrt{\tau_o/\rho_w}$
U <sup>++</sup>	$\int_o^U dU/\sqrt{\tau_o/\rho}$
V	local radial velocity, (ft/hr)
y	distance from wall, (ft)
Y	nondimensionalized distance = y/R
y <sup>+</sup>	$y\sqrt{\tau_o\rho_w/\mu_w/\rho_w}$
y <sup>++</sup>	$\int_o^y \sqrt{\tau_o/\rho/\mu/\rho} dy$
Z	axial coordinate, (ft)

## NOMENCLATURE (Continued)

$\gamma$	local radius, (ft)
$\epsilon_h$	eddy diffusivity of heat, (ft <sup>2</sup> /hr)
$\epsilon_m$	eddy diffusivity of momentum, (ft <sup>2</sup> /hr)
$\mu$	local viscosity, (lbs/ft-hr)
$\mu_o$	reference value of viscosity, (lbs/ft-hr)
$\rho$	density, (lbs/ft <sup>3</sup> )
$\rho_o$	reference value of density, (lbs/ft <sup>3</sup> )
$\tau_o$	wall shear stress (lbs/ft-hr <sup>2</sup> )
$\tau$	local shear stress (lbs/ft-hr <sup>2</sup> )

### Superscripts and Subscripts used

b	refers to bulk mean quantity
w	refers to quantity at wall or wall temperature
o	refers to a reference value of quantity
+	nondimensionalized quantity

## 1. INTRODUCTION

Several supercritical steam generators in the American Electric Power system have shown evidence of tube overheat in the lower furnace at the point where the water bulk temperature is about 670°F. The evidence is of two kinds. First thermal fatigue has occurred and caused tube failures long before a failure of any kind was to be expected. Second, pairs of cordal thermocouples have shown very high wall temperatures and, extrapolating back to the inside of the tube, evidence reduced inside heat transfer coefficients. It was suspected that a possible cause of the high tube temperature was a supercritical "burnout". The primary purpose of this investigation is to determine the cause and conditions leading to a supercritical "burnout" such as might occur in a supercritical steam generator.

Before focusing on this aspect of the problem it is worthwhile to mention several other possible causes for the high tube wall temperatures which have been observed. In this context high means higher than the design temperature. Let us just list these possibilities.

1. Scale inside the boiler tubes.
2. Hot spot factors in the design procedure which are too low.
3. Higher heat transfer from the combustion gases than expected.

Better design procedures or better control of the water purity might be sufficient to cause the problem to disappear without changing the water flow conditions inside the tube.

Because the three factors which are listed above are really rather vague, it appeared that the most promising approach is to eliminate the excessive temperatures inside the tube at supercritical pressure is to eliminate the "burnout". Therefore, only the burnout aspect of the problem has been studied here. The undesirable behavior of the Nusselt number, which is of interest, is indicated in Fig. 1. In particular we want to find out when the supercritical Nusselt number is less than one would expect from the affects of simple property variations alone.

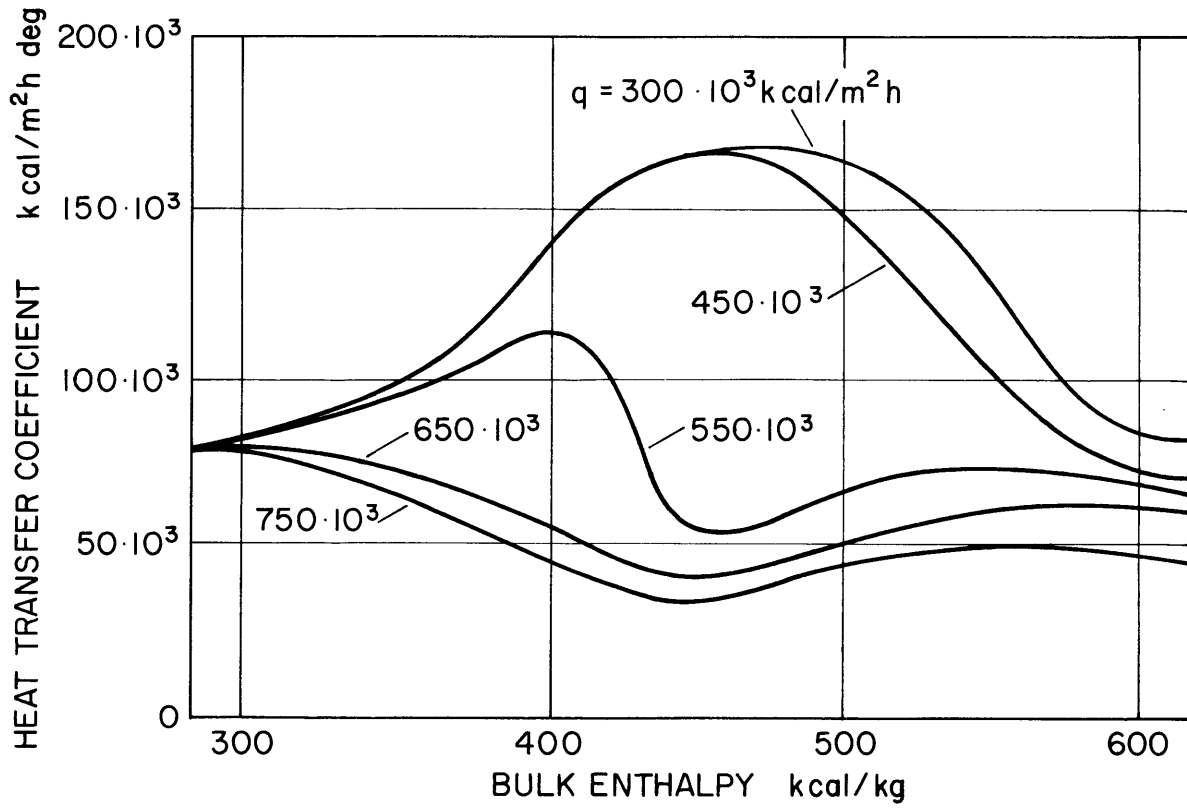


FIG. 1. VARIATION OF THE HEAT TRANSFER COEFFICIENT WITH HEAT FLUX IN THE CRITICAL REGION (FROM REF. 33)

## 2. SCOPE OF PRESENT INVESTIGATION

An experimental and theoretical investigation of the heat transfer at high heat fluxes was undertaken at the Heat Transfer Laboratory at M.I.T. The experimental program was performed with CO<sub>2</sub> as the working fluid because of its convenient critical range.

In general, the methods available for analysis of turbulent flows are either based on the integration of the transport equations with engineering assumptions for the eddy diffusivities of momentum and heat or on integral methods. Often, a Reynolds analogy is useful for correlating the friction factor to the Stanton number.

Another method, frequently used, is to attempt to modify the normal correlations for constant properties by evaluating the dimensionless groups at some reference temperature usually somewhere between the wall and bulk temperatures. In the present instance, it is doubtful whether a reference temperature taken as a fixed linear combination of the wall temperature and bulk temperature will prove useful, because of the nonlinear behavior of the heat transfer coefficient with heat flux.

The method most intensively used in this report is based on the integration of the radial transport differential equations.

### 3. EXPERIMENTAL EVIDENCE OF PREVIOUS INVESTIGATORS

The phenomenon of deteriorated heat transfer at high heat fluxes when transferring heat to a fluid at supercritical pressure has been observed with several fluids by various investigators. The most detailed work is that of Shitsman (1)\* for water. Deterioration has also been reported by Vikrev and Lokshin (2), Shitsman, Miropolskiy and Picus (3), Swenson and Kakarala (4) for water, Powell (5) for oxygen, Szetela (6) in hydrogen and McCarthy (7) in nitrogen tetroxide.

The conditions under which the deterioration was observed to occur are:

1. The wall temperature must be above and the bulk temperature below the pseudocritical temperature.
2. The heat flux must be above a certain value, dependent on the flow rate and pressure.

Figure 2 shows a typically deteriorated region in water from the data of Shitsman (1). The dotted line shows the wall temperature at a flux of 132,000 BTU/ft.<sup>2</sup>-hr. as predicted using the MacAdams correlation ( $NU = 0.023 (Pr)^{0.4} (Re)^{0.8}$ ), in which the bulk temperature is used to evaluate the properties and serves as a reference.

Investigations have shown that the amount of deterioration depends on the inlet enthalpy and pressure (1), and on the orientation of the tube. In particular, the data of Lokshin et al (2) indicates that the deterioration in horizontal tubes is less than and not as sharp as that occurring in vertical tubes for a comparable heat flux. Also, the deterioration in larger tubes has been found to be worse (8).

Similar burnout conditions have been reported in hydrogen and oxygen. In these cases, the rise in temperature has been found to be of even larger magnitude than in water.

---

\* Numbers in paranthesis refer to the References listed on page 57 .

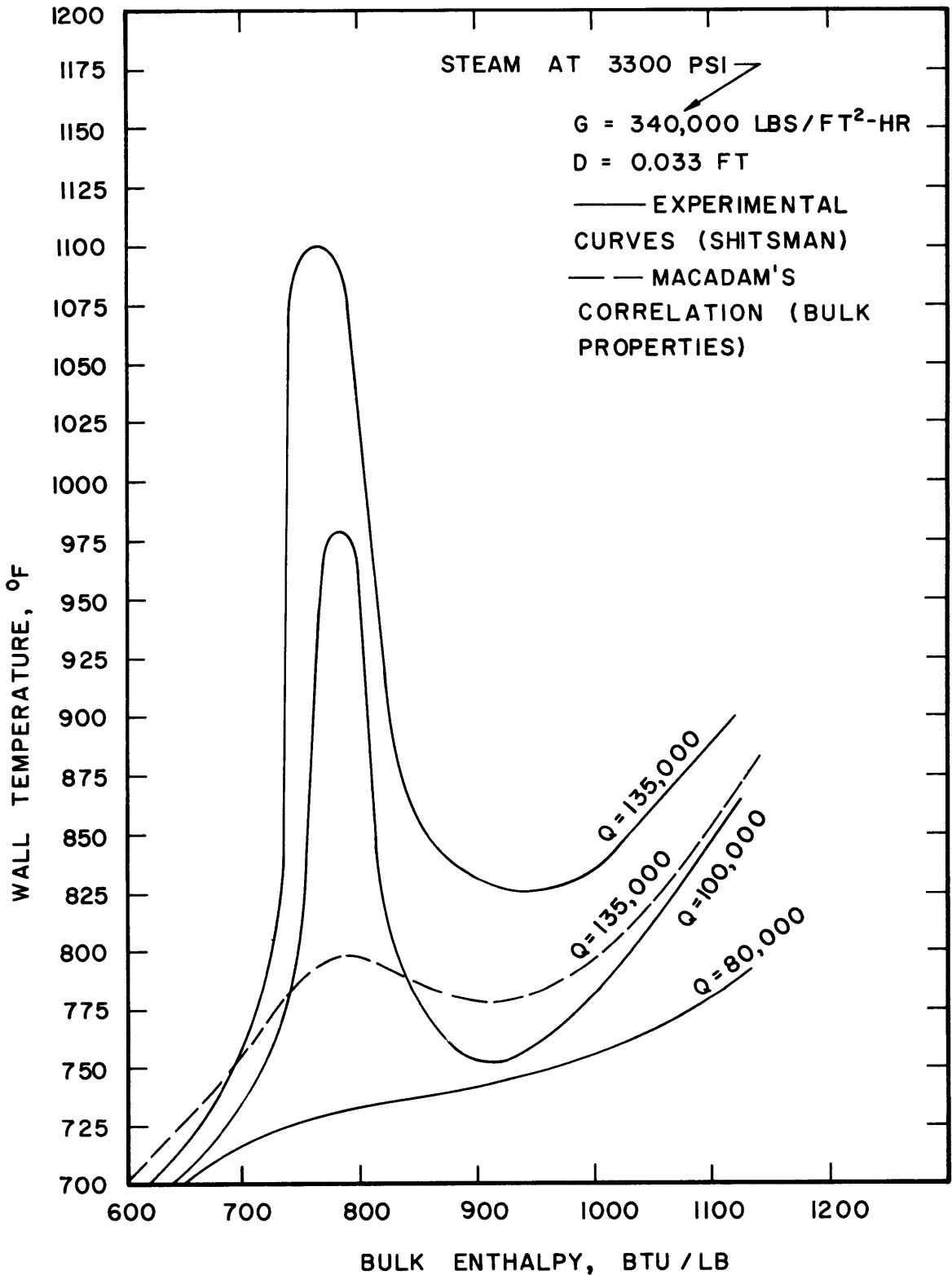


FIG. 2: DETERIORATED HEAT TRANSFER REGION (SHITSMAN)

Though a number of experiments have been done with CO<sub>2</sub> as the working fluid (9, 10, 11, 12, and 13) deterioration has not been observed with CO<sub>2</sub>. However, most of these investigations were at relatively small heat fluxes.

#### 4. PROPERTIES AND THERMODYNAMICS NEAR THE CRITICAL POINT

The reason for the nonlinear behavior of the heat-transfer coefficient with the heat flux is the strong dependence of the properties of the fluid on the temperature in the neighborhood of the critical temperature.

Figure 3 shows the state diagram for  $\text{CO}_2$ , where a constant pressure line at subcritical pressure is represented by 1-1, and at the critical pressure the constant pressure line is represented by 2-2. Assuming thermodynamic equilibrium to exist, an equation for the critical isotherm may be derived by satisfying the conditions for liquid and vapour to co-exist in stable equilibrium with a plane interface in the limiting case. Thus, above the critical pressure, the fluid undergoes no phase transition as it is raised in temperature from below critical to above critical temperature. For the purposes of theoretical analysis in this report, the fluid has been treated on a single phase fluid.

At the critical temperature, the transport properties, viscosity and conductivity, as well as the density, fall sharply, while the specific heat peaks to a high value. Properties of various fluids in the critical region have been investigated and are fairly well known. The properties of water in the critical region were determined by Novak (13), Novak and Grosh (19) etc., and the properties of carbon dioxide were determined by Michels et al (15, 16, 17, 18, and 19), Clark (20), Keesom (21), Tzederberg (22) etc. Figure 4 shows the variation of properties for water at 3300 psi. There has been some controversy regarding the measurement of the thermal conductivity at the critical point. Some investigations report a peak in conductivity at the critical temperature. This has usually been discounted as error in measurement due to thermal convection due to large density differences at the critical point. In this report, the conductivity is assumed to decrease monotonically in the critical region.

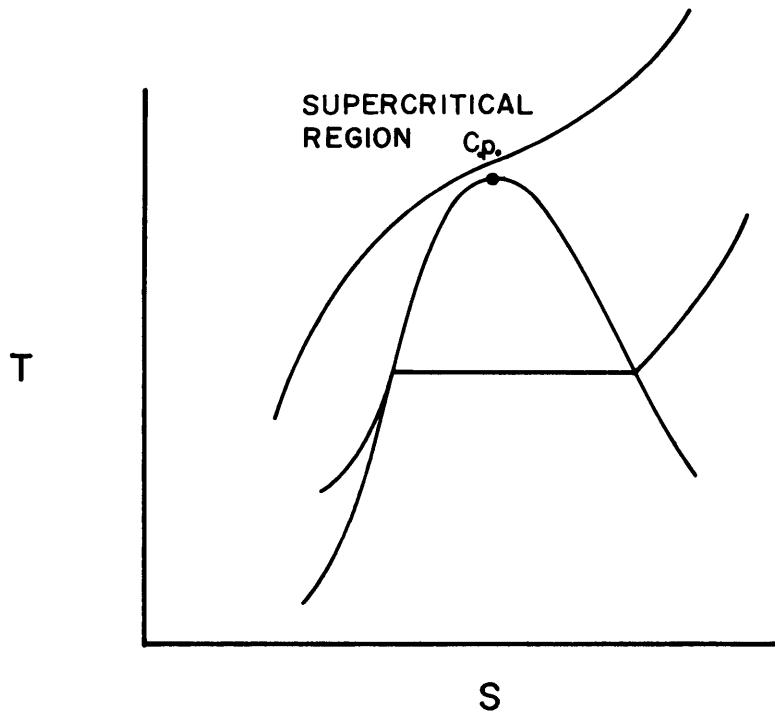


FIG. 3 : STATE DIAGRAM FOR STEAM

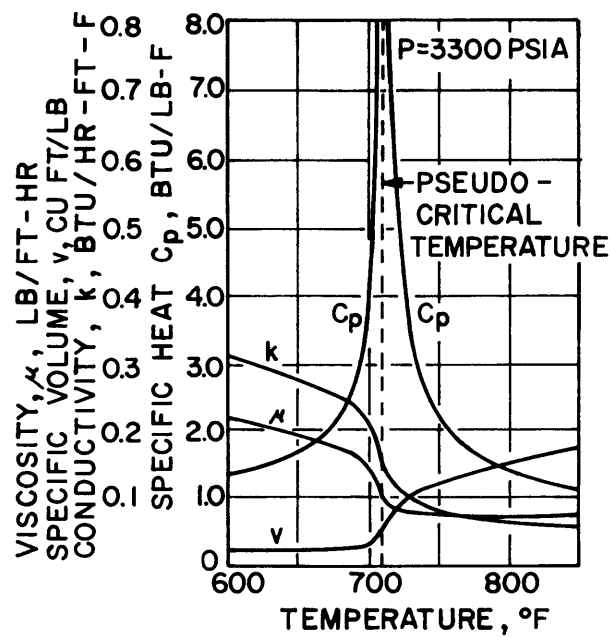


FIG. 4: PROPERTIES OF WATER IN CRITICAL REGION  
(FROM SWENSON & KAKAGRLA)

## 5. THEORETICAL APPROACH

### 1. Introduction

The problem was treated as that of heat transfer to a single phase, turbulent flow with variable properties in order to obtain a theoretical solution. The method used was to solve the simultaneous differential equations governing the momentum and energy balance in the fluid, after making numerous simplifications. The equations were then solved in difference form on the IBM 360 computer at the M.I.T. Computation Center.

### 2. Basic Equations

The equations governing the flow of a fluid through a constant area pipe, in the steady state, and assuming axial symmetry are:

Continuity

$$\frac{\partial(\rho U)}{\partial Z} + \frac{1}{\gamma} \frac{\partial}{\partial \gamma} (\rho \gamma V) = 0 \quad (1)$$

Momentum

$$\frac{\partial \tau}{\partial \gamma} + \frac{\tau}{\gamma} + \frac{dp}{dZ} = 0 \quad (2)$$

Energy

$$\rho C_p \left( U \frac{\partial T}{\partial Z} + V \frac{\partial T}{\partial \gamma} \right) = \frac{1}{\gamma} \frac{\partial}{\partial \gamma} (\gamma q) \quad (3)$$

where

$\gamma$  = local radius

$Z$  = axial coordinate (Fig. 5)

$U$  = local axial velocity

$V$  = local radial velocity

$T$  = local temperature

$\tau$  = local wall shear stress

$dp/dZ$  = pressure gradient in the axial direction

$q$  = local heat flux  
 $\rho$  = local density  
 $C_p$  = local specific heat at constant pressure

This formulation assumes that the momentum terms are small compared to the shear stress and that there is no radial pressure drop, and neglects axial conduction. Also, the momentum equation does not take into account the gravitational term. Hsu (23) has shown that for vertical flow, the effects of free convection are slight in the critical region as long as the Grashoff number is smaller than  $10^{-1}$ .

Furthermore, the transport equations

$$q = - (k + \rho C_p \epsilon_h) \frac{\partial T}{\partial y} \quad (4)$$

$$\tau = (\mu + \rho \epsilon_m) \frac{\partial U}{\partial y} \quad (5)$$

where

$k$  = conductivity  
 $\mu$  = viscosity  
 $\epsilon_h$ , and  $\epsilon_m$  are the eddy diffusivities of heat and momentum  
 must be substituted into the Eqs. (2) and (3) and the resulting equations solved for  $U$ ,  $V$  and  $T$ .

This system of two-dimensional equations can be solved with boundary values specifying the fully developed velocity and temperature profiles at the beginning and end of a long section, together with the boundary conditions  $U = 0$ ,  $V = 0$  at  $y = R$ .

A solution of this type was first attempted with some degree of success, but was given up in favor of a simpler solution which required less time on the computer.

Great simplification is achieved by treating the problem as one of fully developed flow and using only a gross continuity condition over the cross-section.

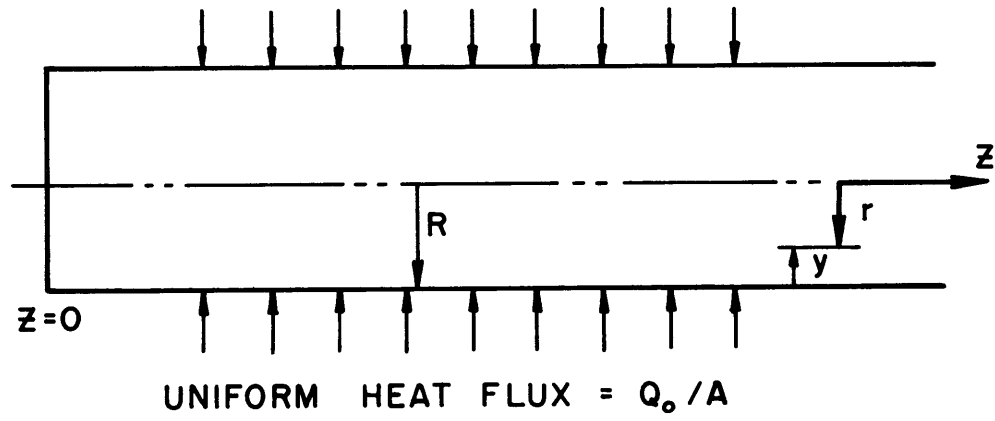


FIG. 5 : COORDINATE SYSTEM FOR FLOW OF FLUID

The simplified system of equations becomes:

Continuity

$$G = \frac{1}{\pi R^2} \int_0^R 2\pi\gamma\rho U dy \quad (6)$$

Momentum

$$\frac{\tau}{\tau_o} = \frac{\gamma}{R} \quad (7)$$

Energy

$$\begin{aligned} \gamma\rho C_p \frac{U\partial T}{\partial Z} &= U\gamma\rho \left| C_p \frac{\partial T}{\partial Z} \right|_{\text{bulk}} \\ &= \rho U\gamma \left| \frac{\partial h}{\partial Z} \right|_{\text{bulk}} = \frac{\partial}{\partial \gamma} (\gamma q) \end{aligned} \quad (8)$$

where

$G$  = mass flow rate/area

$\tau_o$  = wall shear stress

$R$  = radius of tube

Introducing,

$$\left. \frac{\partial h}{\partial Z} \right|_{\text{bulk}} = \frac{\frac{2Q_o}{A}}{GR}$$

where

$Q_o/A$  = wall heat flux/area, the energy equation becomes

$$\frac{\partial}{\partial \gamma} (\gamma q) = \frac{2\gamma\rho U \frac{Q_o}{A}}{GR} \quad (9)$$

which gives the variation of  $q$  along the radius. A still simpler form can be used for the variation of  $q$  by noticing that near the wall  $q = (Q_o/A)$ , and at the center  $q = 0$ . In the central turbulent core, the variation of  $q$  does not influence the results by much. Thus a linear variation in  $q$  may be prescribed

$$\frac{\frac{q}{Q_o}}{A} = \frac{\gamma}{R} \quad (10)$$

Both forms of Eqs. (9) and (10) were tried and the results were found to differ very slightly, hence the simpler form of Eq. (10) was later adopted.

The final simplified equation now becomes

$$\frac{\tau}{\tau_o} = \frac{\gamma}{R} = \frac{R - y}{R}$$

$$\frac{\frac{q}{Q_o}}{A} = \frac{\gamma}{R} = \frac{R - y}{R}$$

$$G = \frac{1}{R^2} \int_0^R 2\rho U(R-y) dy$$

where  $y =$  distance from the wall  $= R - \gamma$  together with the transport equations

$$\tau = (\mu + \rho\epsilon_m) \frac{dU}{dy}$$

$$q = -(k + \rho C_p \epsilon_h) \frac{dT}{dy}$$

which yield

$$\tau = \frac{\tau_o (R - y)}{R} = (\mu + \rho \epsilon_m) \frac{dU}{dy} \quad (11)$$

$$q = \frac{\frac{Q_o}{A} (R - y)}{R} = - (k + \rho C_p \epsilon_h) \frac{dT}{dy} \quad (12)$$

which can be solved simultaneously for U, T with the boundary conditions.

$$y = 0, U = 0, T = T_{\text{wall}}$$

with prescribed wall shear stress  $\tau_o$ , and heat flux  $Q_o/A$ , and when the eddy diffusivities are known.

The mass flow rate and bulk enthalpy at a section are then obtained as:

$$G = \frac{1}{R^2} \int_0^R 2(R - y) U \rho dy \quad (13)$$

$$H = \frac{1}{R^2 G} \int_0^R 2(R - y) U \rho h dy \quad (14)$$

A rudimentary nondimensionalization may be achieved by using reference values of the properties and reference temperature and a reference enthalpy.

$$(1 - Y) = (\mu^+ + \rho^+ \frac{\epsilon_m}{\nu_o}) \frac{dU^+}{dY} \quad (15)$$

$$Q_o^+ (1 - Y) = - \left( k^+ + \rho^+ C_p^+ Pr_o \frac{\epsilon h}{\nu_o} \right) \frac{dT^+}{dY} \quad (16)$$

$$G^+ = 2 \int_0^1 (1 - Y) \rho^+ U^+ \tau_o^+ dY \quad (17)$$

$$H^+ = \frac{2}{G^+} \int_0^1 (1 - Y) \rho^+ U^+ \tau_o^+ h^+ dY \quad (18)$$

where + indicates nondimensionalized values, o indicates reference values

$$Y = y/R$$

$$\mu^+ = \mu/\mu_o$$

$$\rho^+ = \rho/\rho_o$$

$$\nu_o = \mu_o/\rho_o = \text{reference kinematic viscosity}$$

$$U^+ = U\mu_o/R\tau_o$$

$$Q_o^+ = RQ_o/A/T_o k_o$$

$$k^+ = k/k_o$$

$$C_p^+ = C_p/C_{p_o}$$

$$Pr_o = C_{p_o}\mu_o/k_o = \text{reference Prandtl number}$$

$$T^+ = T/T_o$$

$$G^+ = GR/\mu_o$$

$$\tau_o^+ = \tau_o R^2 \rho_o / \mu_o^2$$

$$H^+ = H/h_o$$

$$h^+ = h/h_o$$

with the boundary conditions

$$y = 0, U^+ = 0, T^+ = T^+_{\text{wall}}$$

This formulation has the advantage of eliminating the radius of the tube  $R$  as a separate variable, and reduces the input variables to  $T_{\text{wall}}^+$ ,  $Q_o^+$ ,  $\tau_o^+$  and the output variables to  $G^+$ ,  $H^+$ ,  $T^+$ ,  $U^+$  for a particular pressure.

It should be mentioned that radial integration of this sort has been done before, particularly by Deissler (24). However, it is felt that the type of solution obtained, in terms of quantities nondimensionalized with respect to the shear stress, does not represent the complete solution since the shear stress is not known and cannot be calculated with a constant property correlation. The present solution extends the procedure used by Deissler by solving for the shear stress with the additional constraint by Eqs. (13) or (17).

### 3. Expressions for the Eddy Diffusivity

In order to solve for the velocity and temperature profiles from the preceding equations, expressions for the eddy diffusivities of momentum and heat transfer are required. First of all, it is assumed that the two are equal. Investigations in the past have shown that this is a good assumption when the Prandtl number is not significantly different from unity, and that in this range the ratio of the diffusivities is a weak function of Prandtl number (25).

The best known forms for the eddy diffusivity are due to Deissler (26), van Driest (27) and Spalding (28). Of these, Deissler's is probably the easiest to use and van Driest's the most accurate (29).

For constant property flow, Deissler's expression is

$$\begin{aligned} \epsilon &= n^2 U y & y^+ < 26 \\ &= \frac{k^2 (dU/dy)^3}{\left(\frac{d^2U}{dy^2}\right)^2} & y^+ > 26 \end{aligned}$$

where

$$y^+ = \frac{\sqrt{\frac{\tau_o}{\rho_o}}}{\frac{\mu_o}{\rho_o}} y, \quad n = 0.109, \quad k = 0.36$$

The velocity profiles generated with this expression, match the experimental profiles closely.

For variable property flow, in order to take into account the effect of the local kinematic viscosity, Deissler (24) has suggested the use of the following expression:

$$\begin{aligned} \epsilon &= n^2 U y (1 - e^{-n^2 U y \rho / \mu}) & y^+ < 26 \\ &= k^2 (dU/dy)^3 / (d^2 U / dy^2)^2 & y^+ > 26 \end{aligned}$$

where  $\rho$ ,  $\mu$  are the local properties and  $\rho_o / \mu_o$  are the properties evaluated at the wall temperature.

In the central region  $y^+ > 26$ , it is easier to use Prandtl's expression for diffusivity

$$\begin{aligned} \epsilon &= k^2 y^2 dU/dy \\ k &= 0.36 \end{aligned}$$

Thus, the formulation for the eddy diffusivity becomes (as used by Hsu (23))

Deissler:

$$\left\{ \begin{aligned} \epsilon &= n^2 U^+ y^+ \frac{\mu_o}{\rho_o} \left[ 1 - e^{-n^2 U^+ y^+ \rho_o / \mu_o} \right] & y^+ < 26 \\ &= k^2 \frac{\mu_o}{\rho_o} y^{+2} \frac{dU^+}{dy^+} & y^+ > 26 \end{aligned} \right.$$

Since this formulation involves the use of  $y^+$ ,  $U^+$  based on the properties at the wall temperature, an improvement has been suggested by Goldman (30) in which  $y^+$ ,  $U^+$  are replaced by  $y^{++}$ ,  $U^{++}$

where

$$y^{++} = \int_0^y \frac{\sqrt{\frac{\tau_0}{\rho}}}{\frac{\mu}{\rho}} dy, \quad U^{++} = \int_0^U \frac{dU}{\sqrt{\frac{\tau_0}{\rho}}}$$

so that the expressions for the diffusivity become

$$\text{Goldmann: } \left\{ \begin{array}{ll} \epsilon = n^2 U^{++} y^{++} \frac{\mu}{\rho} \left[ 1 - \exp(-n^2 U^{++} y^{++}) \right] & y^{++} < 26 \\ = k^2 \frac{\mu}{\rho} y^{++2} \frac{dU^{++}}{dy^{++}} & y^{++} > 26 \end{array} \right.$$

The diffusivities suggested by Deissler, Goldman and van Driest were tried and found to yield the same type of results, with differences in wall to center line temperatures of less than 10 per cent. Goldman's scheme has been employed for the bulk of the work since it is more appealing than Deissler's on a physical basis for the reason that it uses an integrated value of the Reynolds number  $y^+$  to determine the transition from the viscous to the turbulent region, rather than  $y^+$  based on the properties at wall temperature.

Several modifications have been suggested in the form of the eddy diffusivity to take into account the presence of large density gradients in the critical region, which tend to promote greater mixing Hsu (23) and Hall (9) suggested multiplying the conventional diffusivity by amplification factors, i. e.

Hsu:

$$\epsilon = \epsilon_{\text{conventional}} (1 + A)$$

$$A = \frac{d(\ln \rho)}{d(\ln C_p T)}$$

Hall:

$$\epsilon = \epsilon_{\text{conventional}} \times C$$

$$C = \frac{B \frac{1}{\rho} \frac{d\rho}{dT}}{\left[ \frac{1}{\rho} \frac{d\rho}{dT} \right]_{T_{\text{standard}}}}$$

where B is a constant to be determined experimentally.

These enhanced diffusivity models suffer from the defect that they lead to enormous diffusivities very close to the wall when the critical temperature is in the vicinity of the wall and yield very large heat transfer rates, irrespective of the magnitude of the heat flux, which is clearly contrary to experiment.

Thus, the diffusivity form suggested by Goldmann has been adopted where

$$y^{++} = \int_0^y \frac{\sqrt{\tau_0}}{\frac{\rho}{\mu}} dy = \sqrt{\tau_0^+} \int_0^Y \frac{\rho^+}{\mu^+} dY$$

$$U^{++} = \int_0^U \frac{dU}{\sqrt{\frac{\tau_0}{\rho}}} = \sqrt{\tau_0^+} \int_0^{U^+} \sqrt{\rho^+} dU$$

in terms of previously nondimensionalized quantities where

$$\tau_0^+ = \frac{\tau_0 R^2 \rho_0}{\mu_\tau^2}, \quad U^+ = \frac{U \mu_0}{R \tau_0}$$

#### 4. Method of Solution

The solution consists in numerically solving the Eqs. (11) and (12) (using the expressions for eddy diffusivity in the previous section) for a prescribed heat flux  $Q_o/A$ , shear stress and wall temperature and then evaluating the mass flow rate and bulk enthalpy from the integrals in Eqs. (13) and (14). The method used was an explicit finite forward difference procedure, starting at the wall and proceeding inwards to the center of the tube. Because of the large amount of calculation involved in computing the profiles for various wall temperatures and wall shear stresses, this method was preferred as being the quickest over a formal relaxation procedure, though it is less accurate. By using a first order difference procedure which yields a positive error in the bulk velocity and temperature drop and a second order procedure, which yields a negative error, bounds can be placed on the solution. For constant properties, the solution checks with known results to within 2 per cent.

Thus, the essentials of the solution can be tabulated in the following way:

$Q_o/A$	$T_{\text{wall}}$	$\tau_o$	T	U	G	H
50,000	800	$2 \times 10^7$	800	0	$4 \times 10^5$	685
			798	200		
		$3 \times 10^7$	800	0	$4.5 \times 10^5$	705

## 5. Results

The bulk of the results are presented in the form  $G^+$  versus  $H^+$  for different wall temperatures and heat flux parameter  $Q_o^+$ . In order to feed in the properties without reducing them by division by standard quantities, it was found convenient to designate the value of unity to all reference quantities

$$\begin{aligned}\rho &= f(T) \text{ can be represented numerically by} \\ \rho/\rho_o &= f(T/T_o) \text{ etc.} \\ G^+ &= GR/\mu_o \text{ represents the numerical value } GR \\ Q_o^+ &= (Q_o/A)R/T_o k_o \text{ represents the numerical value } Q_o/A \times R \\ \tau_o^+ &= \tau_o R^2 \rho_o / \mu_o^2 \text{ represents the numerical value } \tau_o R^2\end{aligned}$$

Figures 6, 7, 8 and 9 are plots of GD versus H for different wall temperatures for three different values of the heat flux parameter  $QD = 3300, 5000, 15000, 25000$  BTU/ft.-hr. The GD range in each plot is such that it shows the region of interest, where hot spots are likely to occur. The peak and dip in the isotherms correspond to the maximum flow rate (in the pre-critical enthalpy region) and the minimum flow rate possible at that temperature, respectively. These represent the point of the maximum temperature for the first flow and the minimum temperature for the second flow rate respectively.

In order to use these plots for a particular problem, it is necessary to make a crossplot of wall temperature versus bulk enthalpy for a constant flow rate. Figure 10 shows crossplots made for  $G = 340,000$  lbs/ft.<sup>2</sup>hr. for three heat fluxes,  $Q = 80,000, 100,000, \text{ and } 132,000$  BTU/ft.<sup>2</sup>-hr for a tube of diameter 1/30 ft. in order to compare these results with the experimental results of Shitsman(1). This plot corresponds to the variation of wall temperature along the length of a tube with uniform heat input. It is seen that the calculations predict a marked deterioration in heat transfer at about the same heat flux observed experimentally. It is also evident that the predictions are somewhat high in the region beyond the peak. This is probably due to the fact that there is additional mixing in this region of large density gradients in the core, which has not been taken into account in the calculations. Also this is the region where the fully developed profile assumptions are least valid.

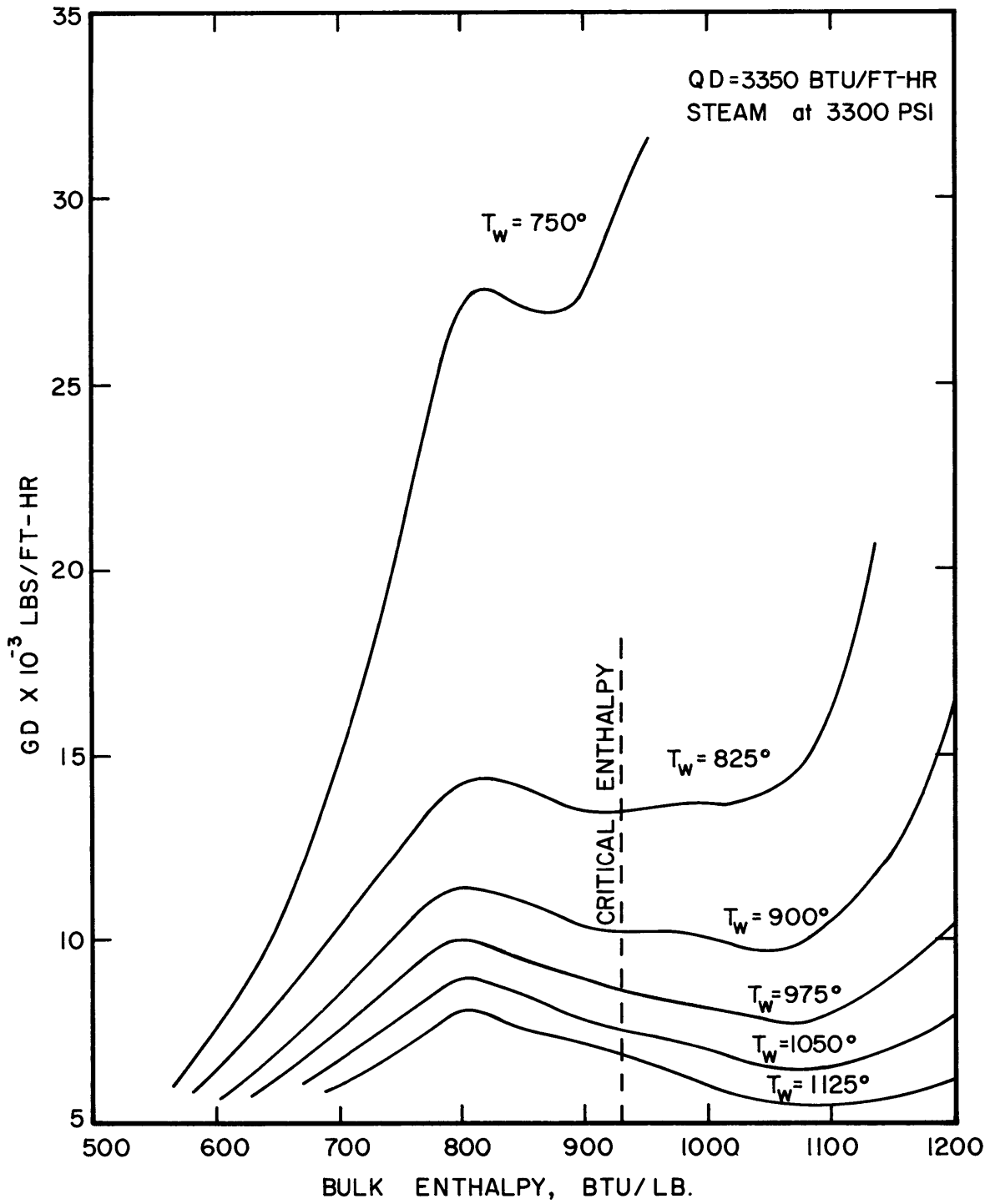


FIG. 6 : COMPUTED RESULTS : MASS FLOW RATE VS. BULK ENTHALPY FOR SYSTEM

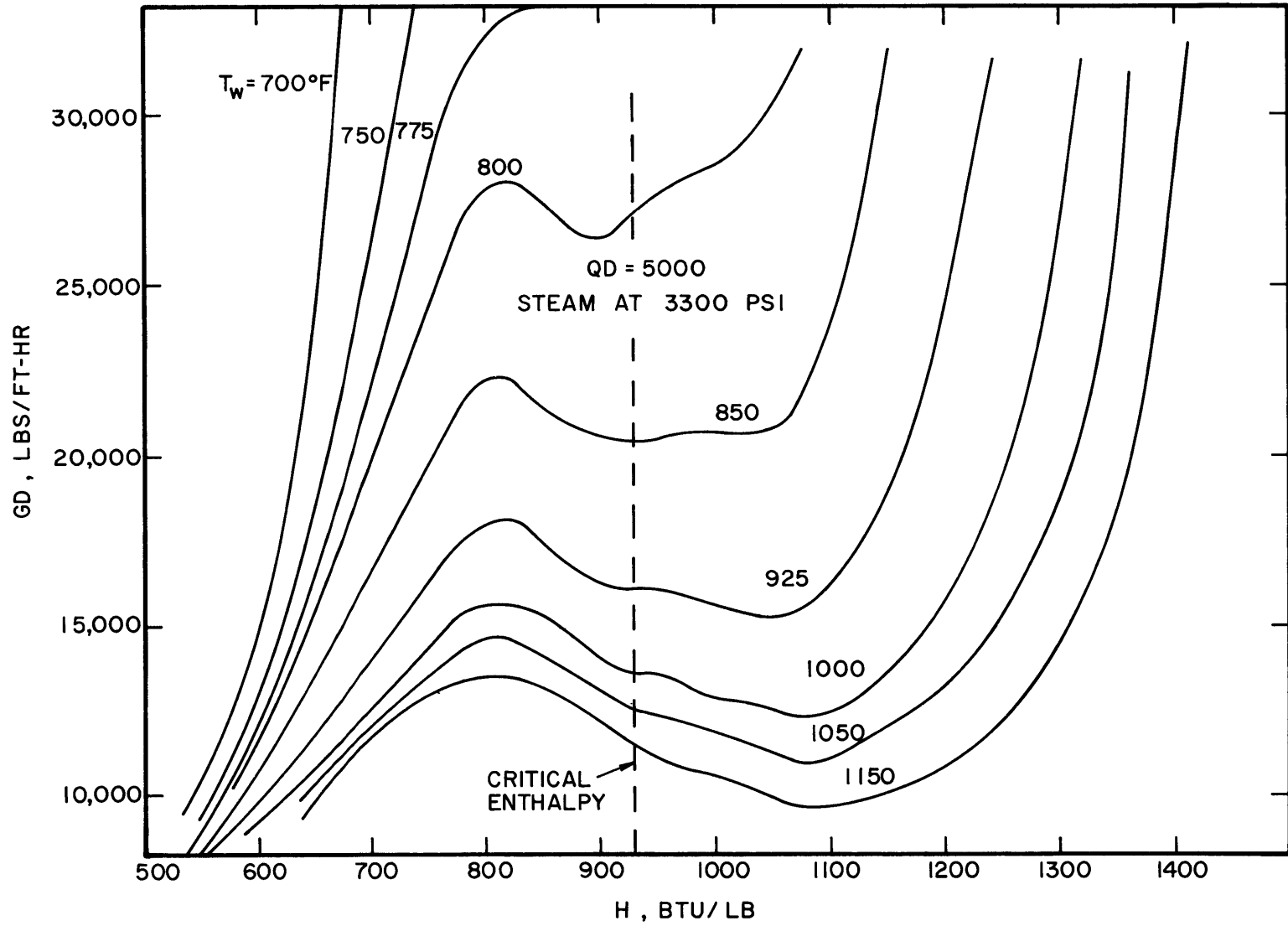


FIG. 7 : COMPUTED RESULTS : MASS FLOW RATE VS. BULK ENTHALPY FOR SYSTEM

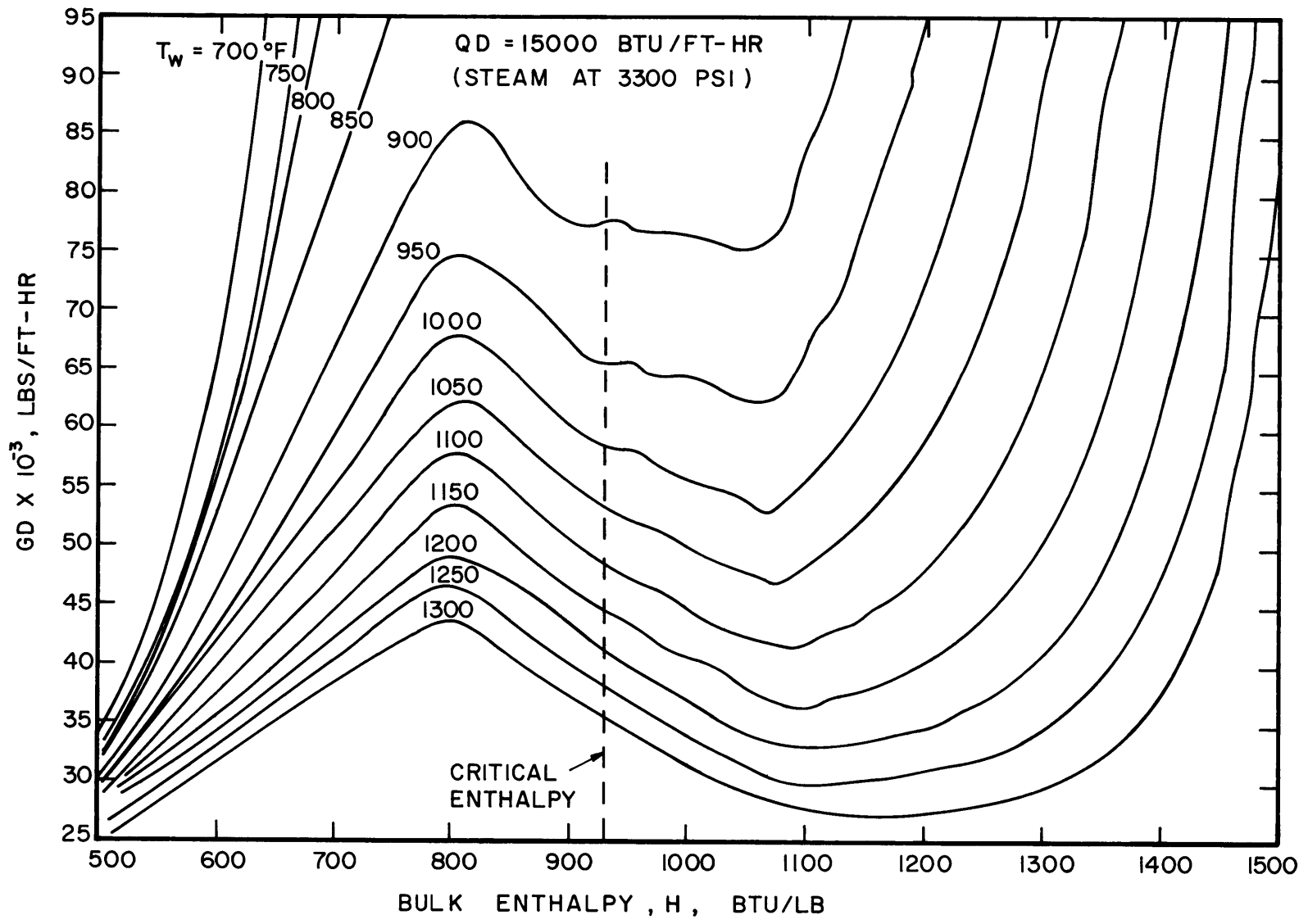


FIG. 8 : COMPUTED RESULTS : MASS FLOW RATE VS. BULK ENTHALPY FOR SYSTEM

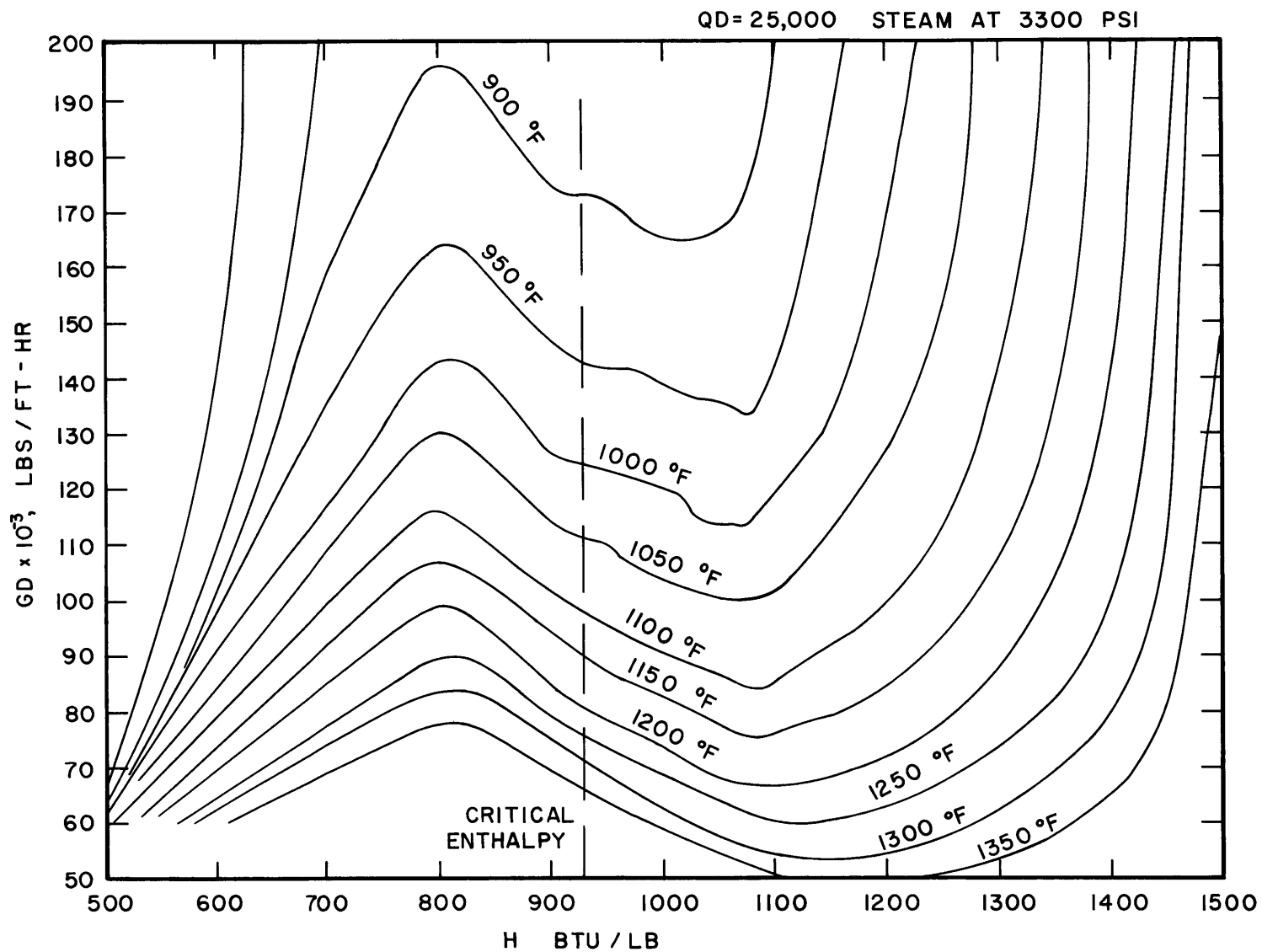


FIG. 9 COMPUTED RESULTS: MASS FLOW RATE VS. BULK ENTHALPY FOR STEAM

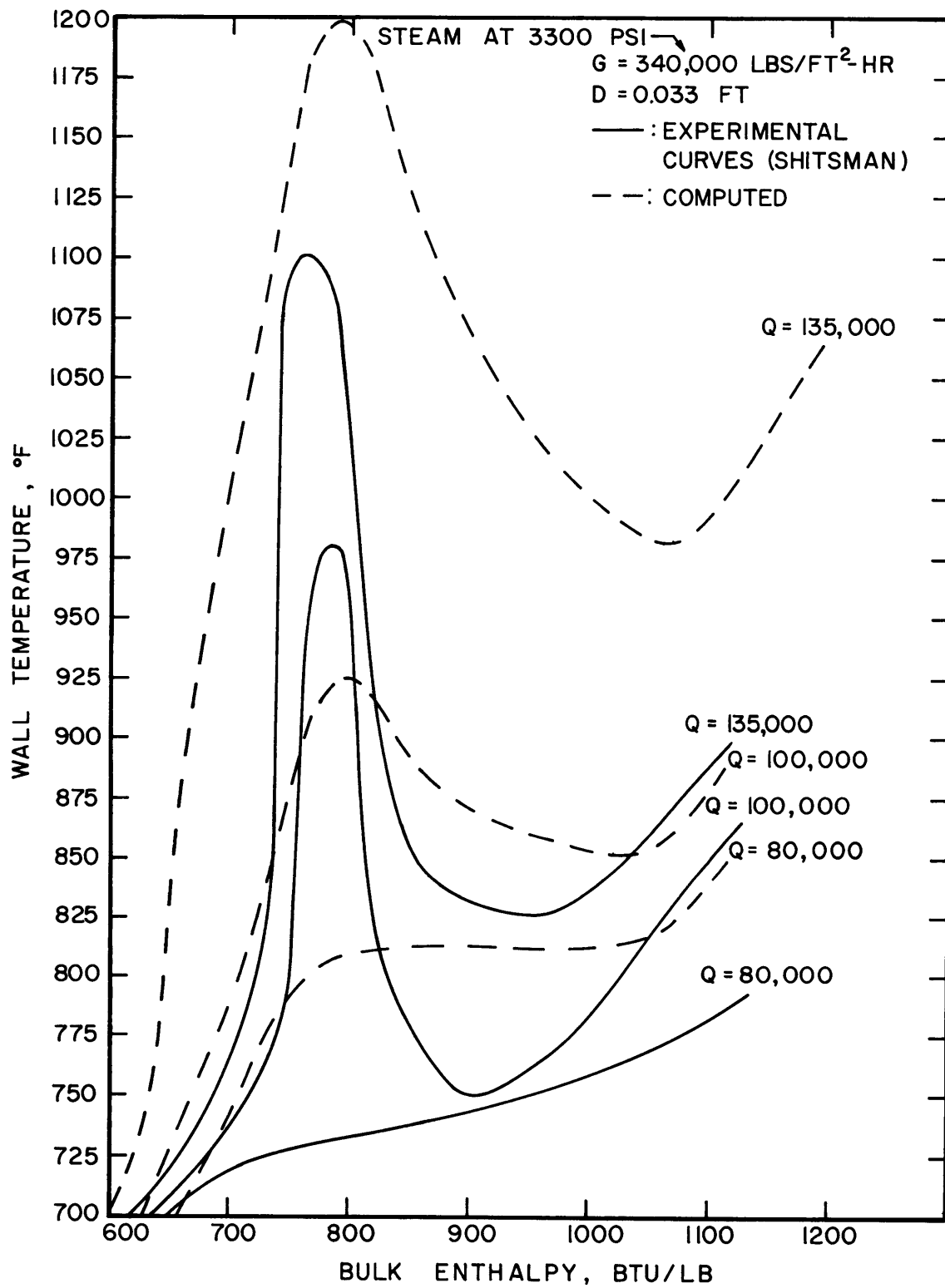


FIG. 10 : DETERIORATED HEAT TRANSFER REGION (SHITSMAN)

Since the variation of shear stress along the length is an important part of the solution, a sample plot of GD versus enthalpy is shown in Fig. 11 for various values of  $\tau_o$ . A crossplot of shear stress versus enthalpy (Fig. 12) shows that the shear stress dips before rising to a higher value corresponding to the gaseous state. An examination of the effect of heat flux shows that the dip gets more pronounced at a higher value of the heat flux.

Figures 13, and 14 show typical velocity and temperature profiles at different sections of the tube, corresponding to the deteriorated region and regions in the liquid and vapors regimes, away from the critical point. The temperature drop in the region close to the wall is proportionately larger in the deteriorated region. An explanation, sometimes suggested for the deterioration phenomenon, is that 're-laminarization' of the boundary layer takes place. Though this is confirmed by this investigation to the extent that there is a drop in the shear stress, the velocity profiles do not tend towards the conventional laminar velocity profiles. The drop in shear stress is largely due to the drop in density and viscosity near the wall, without an appreciable increase in the core velocity.

The locus of the critical temperature is of some interest, for example, in the formulation of integral methods of solution. Figure 15 shows that the locus is 'flatter' than for a constant property flow, i.e., the critical temperature persists longer near the wall.

## 6. Simplified Physical Model

It is possible to postulate a simple physical model to explain the deterioration phenomenon, based on the evidence of the computed results.

If the equations governing the flow are examined,  $(1-Y) q_o = -\rho(k/\rho C_p + \epsilon_h) dh/dY$ ,  $(1-Y)\tau_o = \rho(\mu/\rho + \epsilon_m) dU/dY$ . It is evident that the velocity profiles and enthalpy profiles will be identical if the molecular Prandtl number  $C_p\mu/k$  and the turbulent Prandtl number  $\epsilon_m/\epsilon_h$  are both unity.

Since the assumption that  $\epsilon_m = \epsilon_h$  has been made, and the Prandtl number  $C_p\mu/k$  does not differ largely from unity except in small regions, it should be expected that the relation

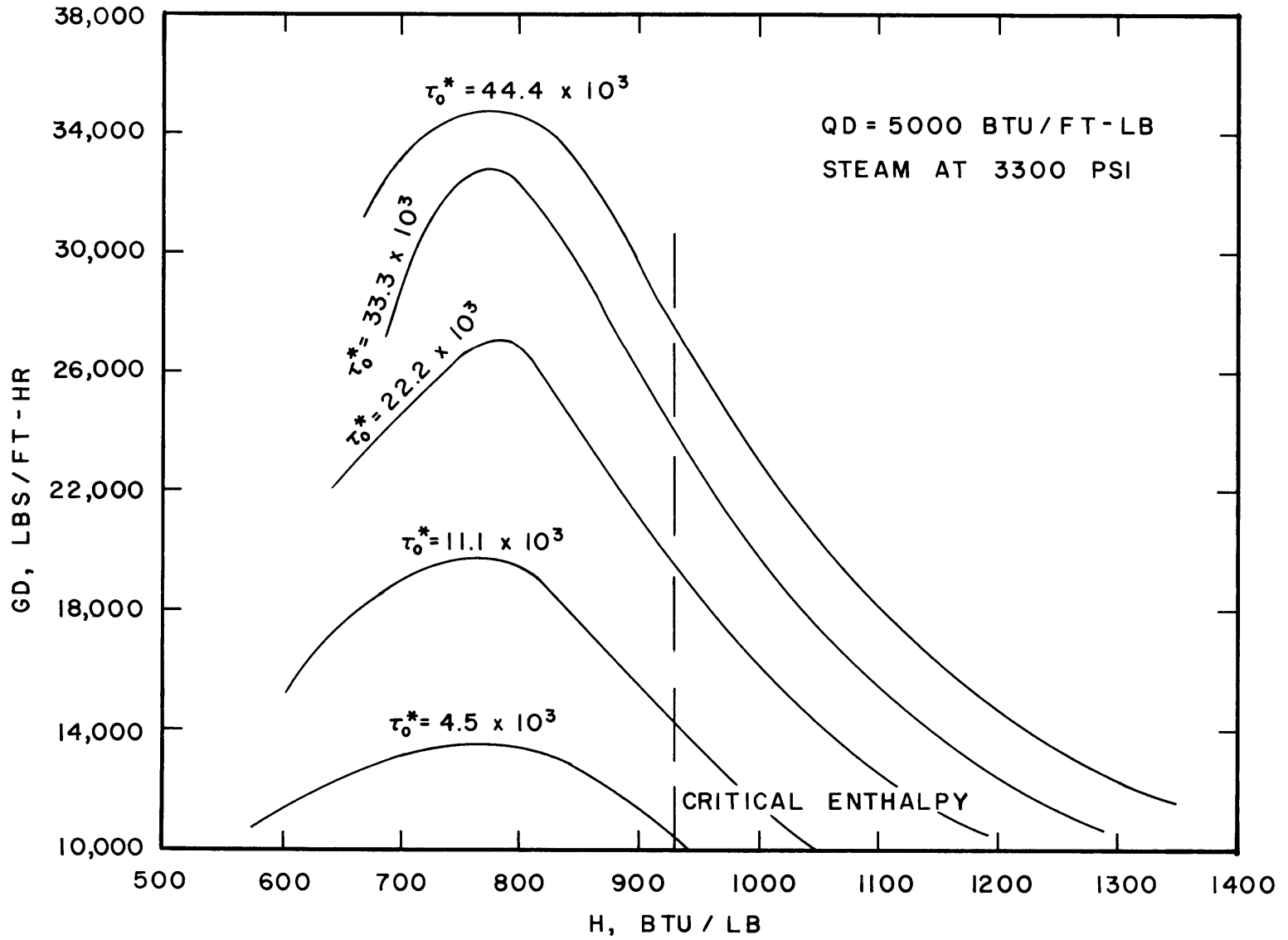


FIG. II COMPUTED RESULTS : CONSTANT SHEAR STRESS LINES

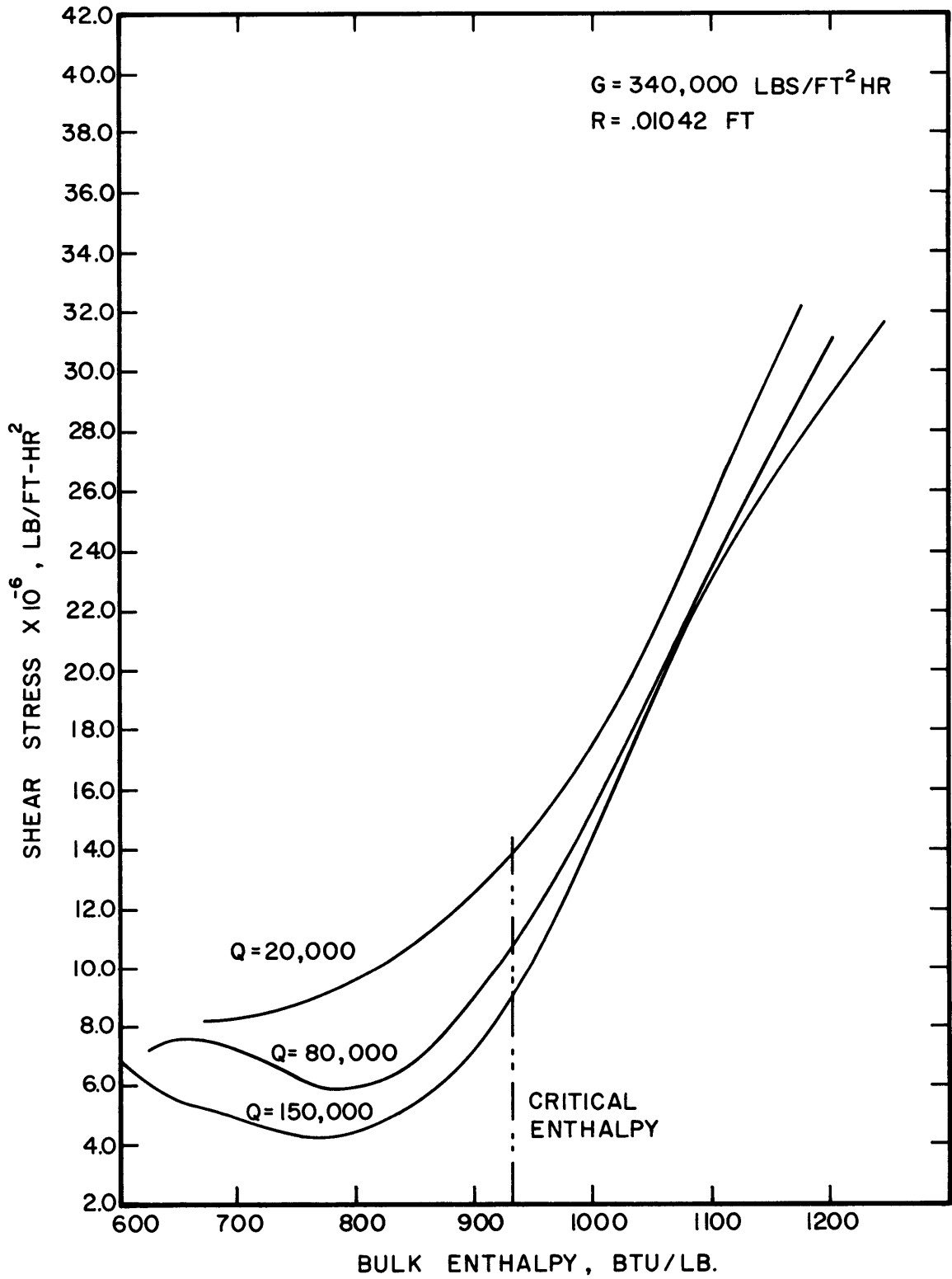


FIG. 12 : VARIATION OF SHEAR STRESS WITH HEAT FLUX

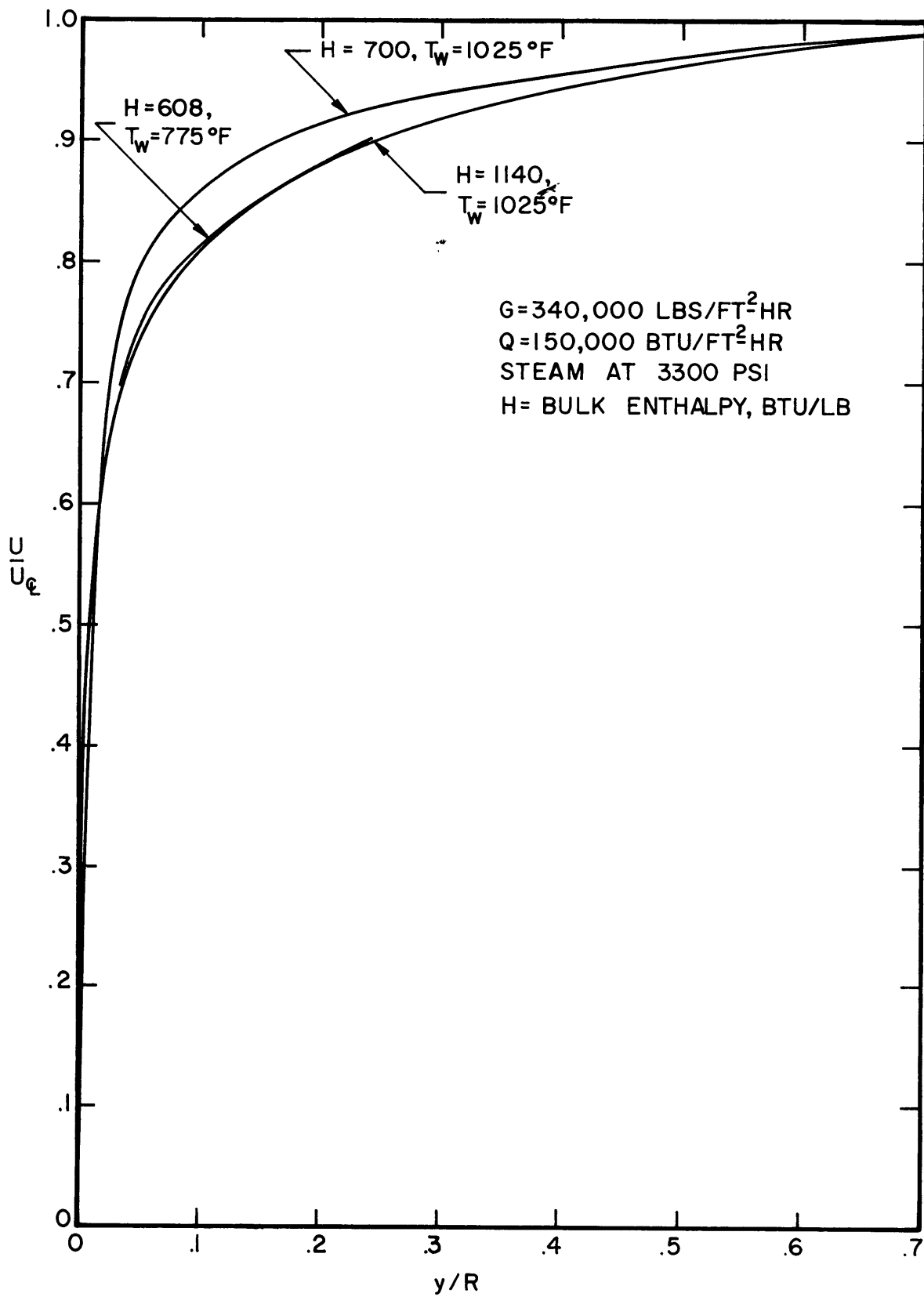


FIG. 13: COMPUTED VELOCITY PROFILES

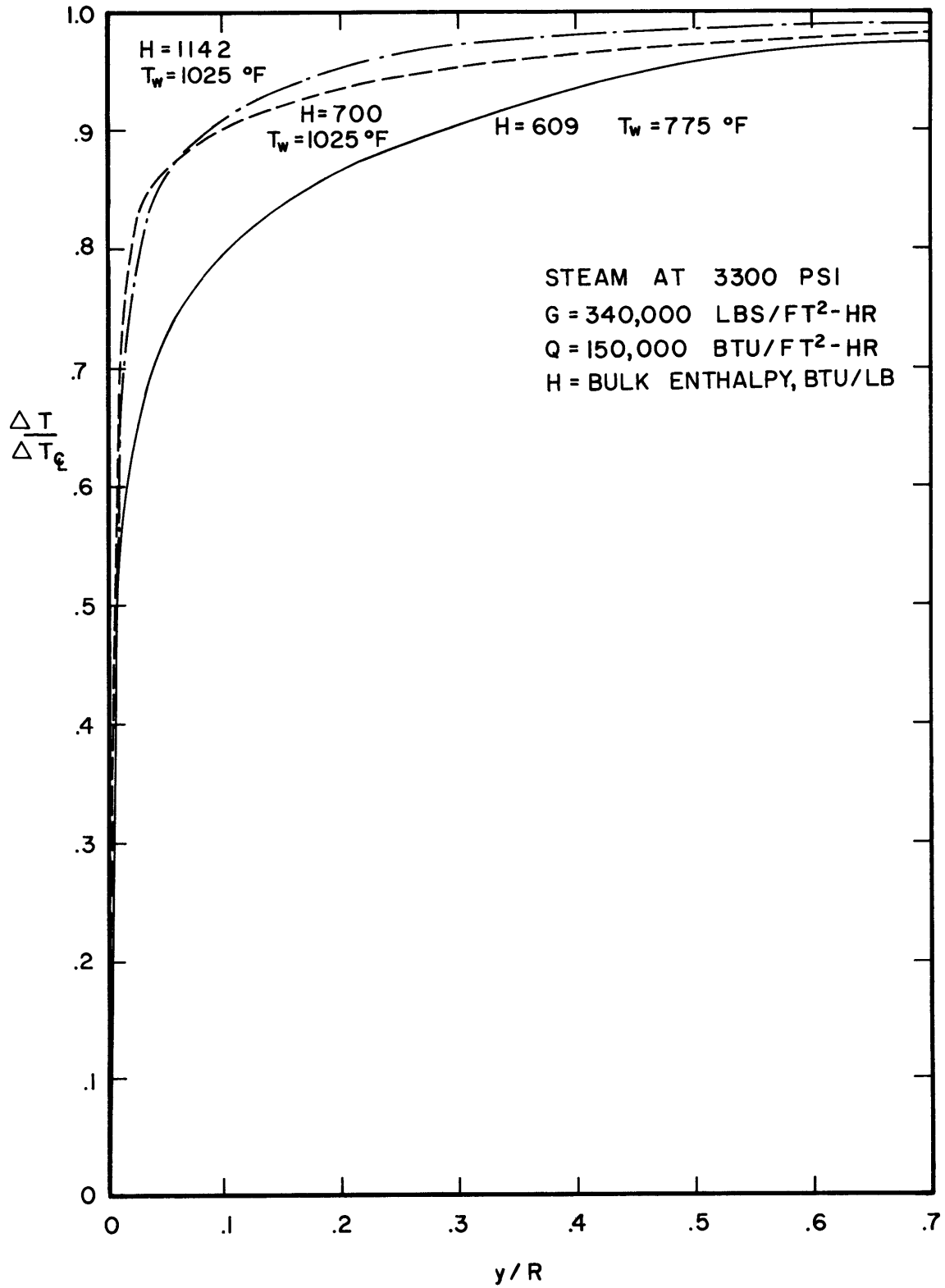


FIG. 14 COMPUTED TEMPERATURE PROFILES

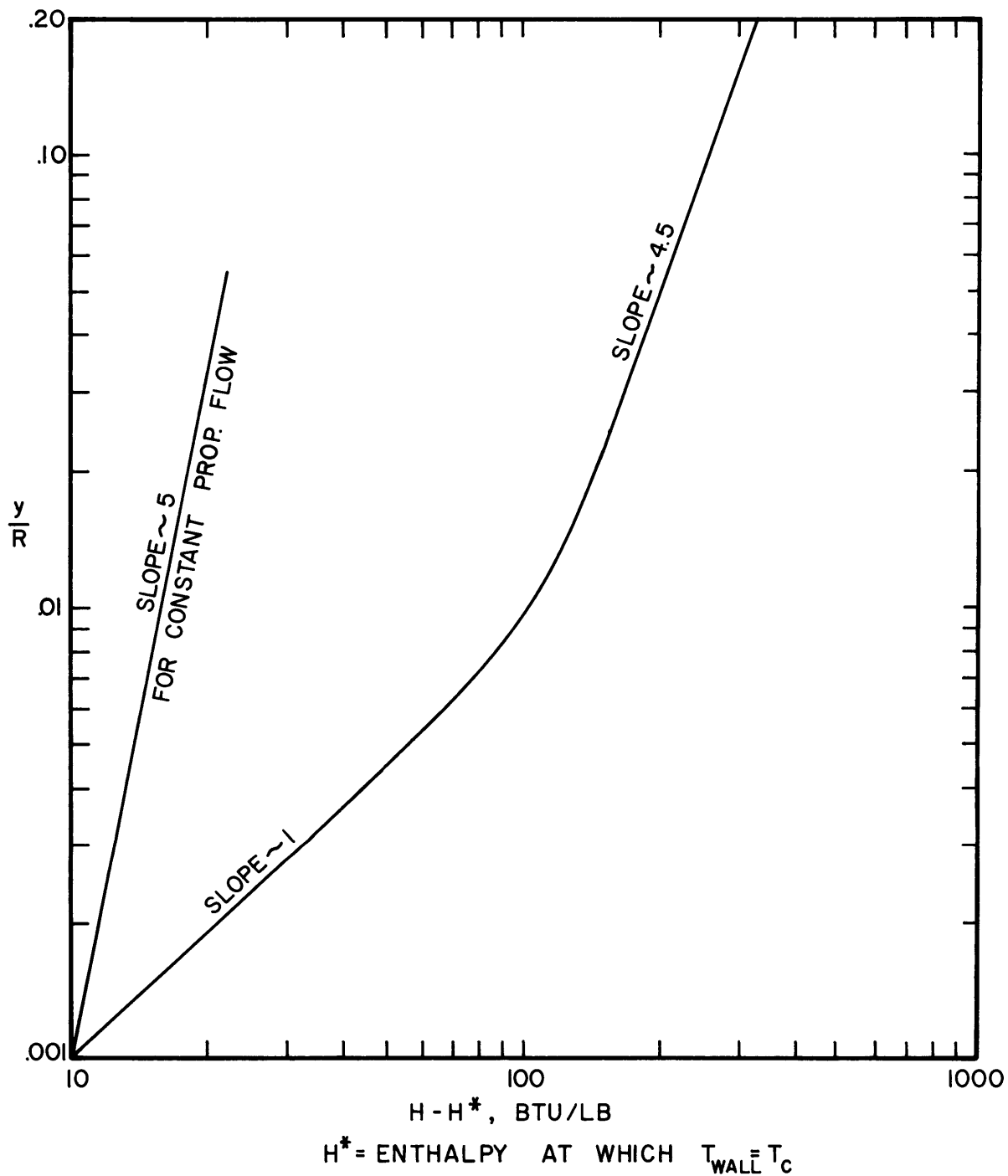


FIG. 15 : RADIAL LOCUS OF  $T_c$  IN A TYPICALLY DETERIORATED REGION

$$\frac{q_o}{\tau_o} = \frac{\Delta h}{\Delta U}$$

will hold in the pre-critical enthalpy region.

or

$$\frac{q_o}{\Delta h \rho_b U_b} = \frac{\tau_o}{\rho_b U_b^2} \quad (19)$$

which is Reynolds analogy with the enthalpy drop  $\Delta h$  used instead of  $C_p \cdot \Delta T$ . Thus, there is a good correlation between the friction factor and the heat transfer rate, and the deterioration in heat transfer corresponds to the drop in shear stress.\* The drop in shear stress is basically governed by the radial temperature drop in the fluid stream as it approaches the critical region. When there is sufficiently large temperature difference between the wall and the bulk of the fluid, with the wall temperature being higher than the critical temperature and the bulk temperature below it, the bulk velocity is essentially that of the high density fluid whereas the fluid near the wall is of low density. This causes the shear stress, governed by  $\rho \overline{\mu'v'}$  to drop by a substantial amount.

Furthermore, along the tube as the bulk enthalpy reaches a value equal to the critical enthalpy, there is an improvement in heat transfer due to increased shear stress and turbulence, a high value of the bulk Prandtl number and enhanced mixing.

Thus, the phenomena of deterioration and improvement in heat transfer always exist side by side. At low heat fluxes, the deterioration is wiped out due to the nearness of the bulk temperature to the wall temperature, since the reduced viscosity and density in the film is almost simultaneously accompanied by increased velocities, and an increase in  $\rho C_p$  in the core of the flow.

The situations in the case of low and high heat fluxes are illustrated in Fig. 16.

---

\* Recent checks have shown that Eq. (19) is not very good in the region of the temperature peak, due to the high Prandtl number near the wall, and that the deterioration in the heat transfer is greater than the drop in shear stress.

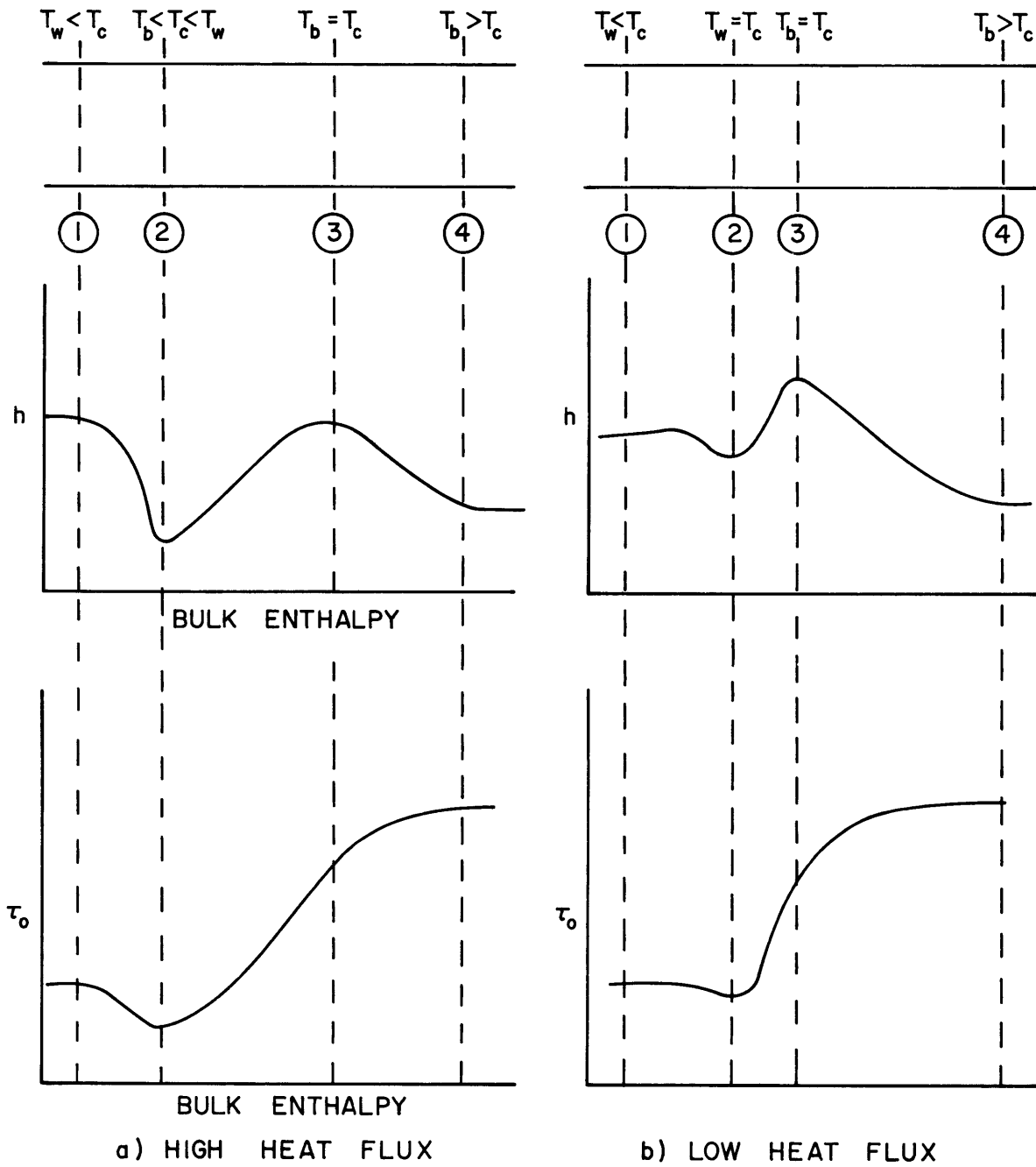


FIG. 16 : PHYSICAL EXPLANATION OF HEAT TRANSFER VARIATION

## 7. Safe Versus Unsafe Plot for Steam

Since the computed results indicate an almost continuous progressive deterioration in heat transfer as the heat flux is increased, it is necessary to make a somewhat arbitrary decision as to when the deterioration is unsafe. For this purpose it was decided to use the following simple criterion. The heat flux is unsafe if in the region where

$$T_{\text{bulk}} < T_c < T_{\text{wall}}, \quad \frac{\text{Nu}_{\text{mac}}}{\text{Nu}} > 2$$

where

$$\text{Nu}_{\text{mac}} = 0.023 (\text{Re})^{0.8} (\text{Pr})^{0.4}$$

Re, Pr based on properties at the bulk temperature

Nu = computed Nusselt number

With this definition, it is possible to make a safe versus unsafe plot for steam in terms of the heat flux versus mass flow rate. This is shown in Fig. 7. Here, if the conditions in terms of heat flux and flow rate correspond to a position above the line, the temperature rise is unsafe. Comparison with experimental points of Shitsman(1) has shown that a prediction on this basis tends to be slightly conservative.

In a recent paper by Styrikovich (33) design considerations for supercritical boilers have been presented based on experimental data. The authors suggest on an experimental basis that the deterioration in heat transfer approximately corresponds to the conditions  $G/Q_o/A < 4$  lbs/ft.<sup>2</sup>-hr/BTU/ft<sup>2</sup>-hr and give 'allowable heat fluxes' for tubes 5 mm.-in. diameter. These are shown in Fig. 17. Curve 2 corresponds to a constant external tube surface of 580°C (1000°F) and curve 3 is for local thermal loads in the lower radiant section when the boiler operates on gas. The computed curve compares favorably with the experimental criteria.

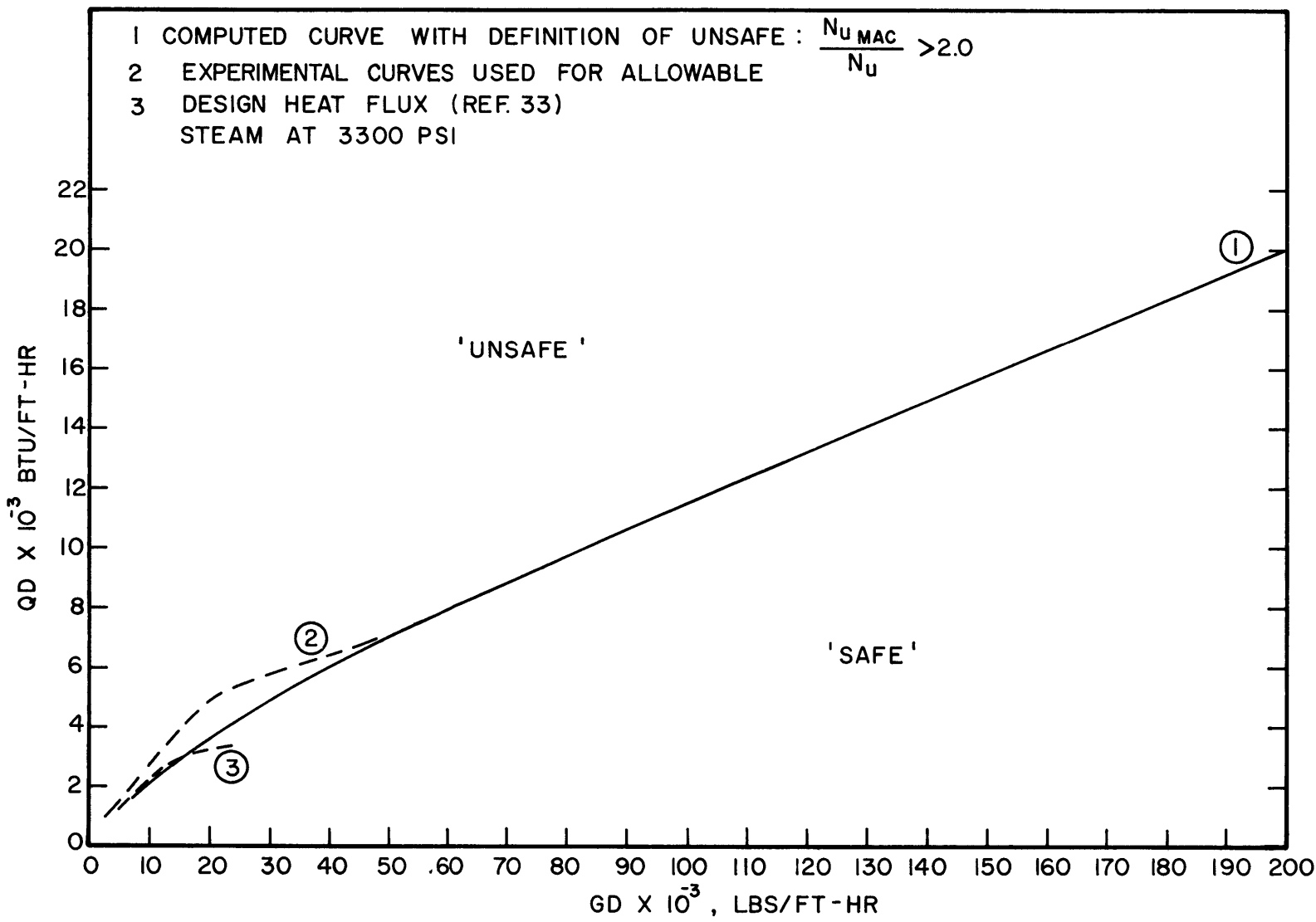


FIG. 17 : COMPUTED SAFE VS. UNSAFE PLOT FOR SYSTEM

## 6. EXPERIMENTAL APPROACH

### 1. Introduction

A detailed experimental program was undertaken to verify the computed results. Carbon dioxide was used as the working fluid because of its convenient properties ( $T_c = 88^\circ \text{F}$ ,  $p_c = 1071 \text{ psi}$ ) as compared to those of water ( $T_c = 705^\circ \text{F}$ ,  $p_c = 3206 \text{ psi}$ ). Carbon dioxide has been used for supercritical pressure studies by various investigators for the same reasons. These include the work of Hall, Jackson et al (19), Knapp and Sabersky(31), Koppel and Smith (11), Tanaka (12) etc. None of these investigators have reported sharp deterioration patterns as in other fluids. The reason may be that Hall, Knapp, and Tanaka did not use high enough heat fluxes, while Koppel and Smith though using a wide range of heat fluxes, did not have low enough inlet temperature to observe the deterioration effects. The deterioration in carbon dioxide which was observed to be present in the present investigation, has been found to be very sensitive to the inlet enthalpy, as well as such factors as swirl due to upstream disturbances, test section vibration and scale formation in the heater.

### 2. Description of Apparatus

The experimental setup (shown in Fig. 18), consists of a closed circulation loop in which the system pressure is maintained with a hydraulic accumulator, using high pressure nitrogen gas. A centrifugal pump is used to circulate the carbon dioxide in the loop, thus minimizing the possibility of large pressure variations and oscillations in the system. The test section of stainless steel is vertical, 1/4 in. on the inside diameter and 3/8 in. on the outside diameter, and 5 ft. long. The section is heated electrically with a D-C power supply consisting of a motor-generator unit capable of about 12 kw. Initially the test section was clamped between the electrodes, but was later provided with a floating support to eliminate vibration, induced due to thermal expansion and bowing. The plumbing is arranged so that the flow can be either up or down in the test section. About a foot of unheated length of tubing ( $L/D = 50$ ) is provided at each end of the heated section. Fourteen thermocouples (30 gauge copper-constantan) are located along the length of the test section, at intervals of 3 in. in the center of the tube and

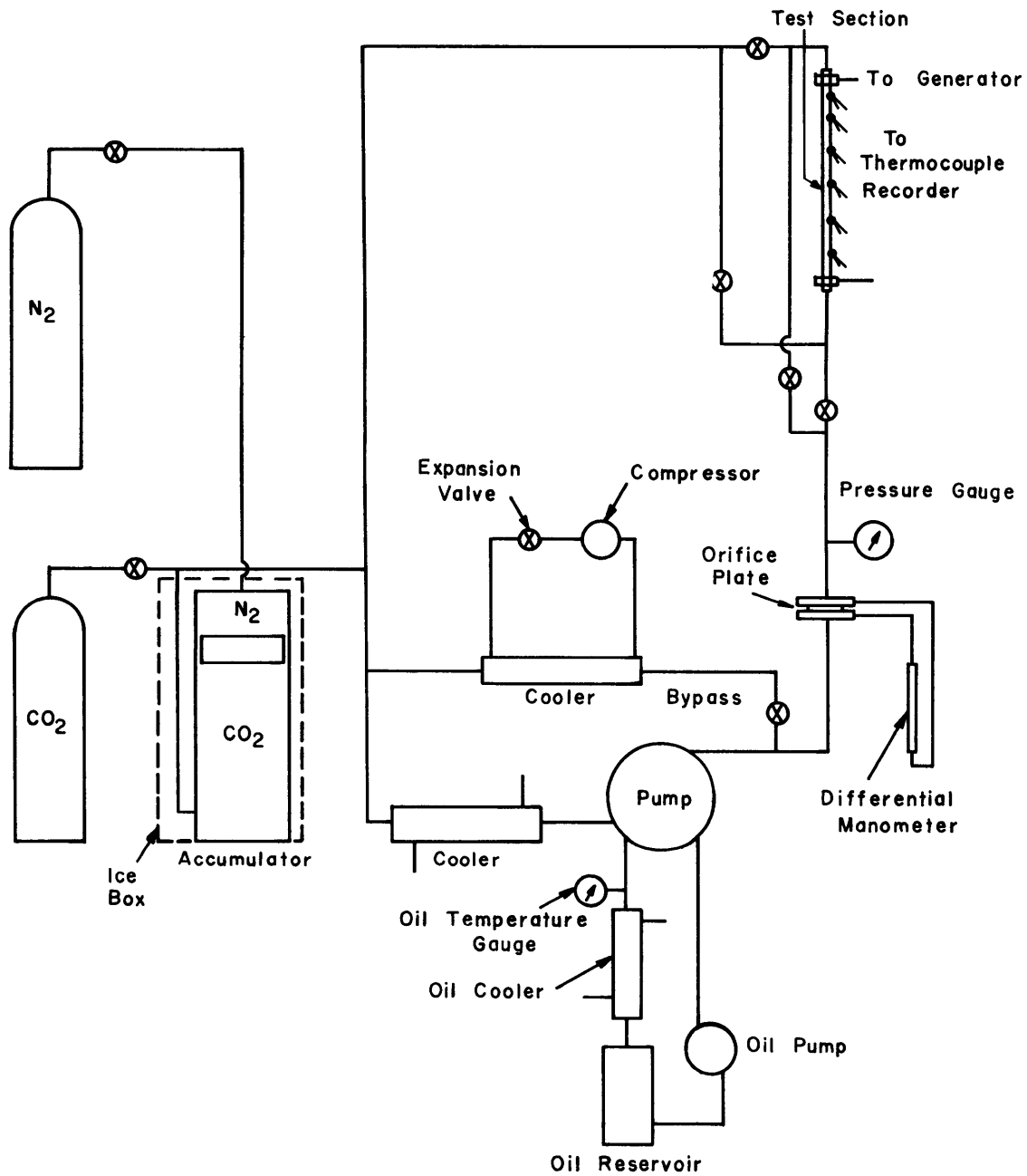


FIG. 18 SCHEMATIC DRAWING OF EXPERIMENTAL LOOP

4 in. - 6 in. near the ends. The thermocouples are mounted on thin mica insulators because D-C heating is employed. The inlet and outlet fluid temperatures are measured by inserting two thermocouples into the fluid at the entrance and exit of the test section. The thermocouple output is recorded on a chart recorder type of potentiometer, which records the output of the 16 thermocouples in succession. The system pressure is measured by means of a Heise-Bourdon gauge, calibrated from 0 to 2000 psi in intervals of 2 psi.

The flow is monitored by means of a calibrated orifice plate with flange pressure taps. The pressure drop across the orifice is measured by a 5 ft. differential manometer capable of sustaining 2000 psi internal pressure.

Initially, only a cold water once-through heat exchanger was employed for cooling, but later a refrigeration unit was added to the pump bypass loop since greater inlet subcooling was found to be necessary.

The carbon dioxide was obtained from Liquid Carbonic Division of General Dynamics and is 99.9 per cent pure.

### 3. Capabilities and Measurements

The pump is capable of supplying flow rates of up to  $2 \times 10^6$  lb/ft.<sup>2</sup>-hr to the test section. The inlet fluid temperature at steady state can be kept as low as 30°F. The power supply is capable of about 12 kw corresponding to a heat flux of about 120,000 BTU/ft.<sup>2</sup>-hr. on the inside diameter of the test section. The measurements made in each run were:

- a. The heat flux, calculated from the power input, recorded by measuring the current in the test section and the voltage drop across it (within 1 per cent).
- b. The pressure at the test section inlet measured by the Heise Gauge, within 1 psi. The pressure drop within the test section was not measured, but calculated to be of the order of 1 psi or less.
- c. The flow rate measured by recording the pressure drop across the orifice plate (accuracy 1 per cent of full scale reading.)

- d. The inlet and outlet fluid temperatures and fourteen thermocouple readings along the wall, correct to one degree F.

Heat balance checks were run on the loop at a pressure of 1200 psi and by arranging the flow and heat flux so that the inlet and outlet temperatures were not in the critical range. The heat balance was found to be good within 5 per cent.\*

Most of the data was taken at the slightly supercritical pressure of 1100 psi. Some data was also taken at 1150 psi. The procedure consisted in fixing the heat flux and taking data at various flow rates.

#### 4. Experimental Results

The results from the experiments were obtained in the form of wall temperature profiles as a function of the length along the test section, and therefore, of the bulk enthalpy. The inner wall temperature was calculated assuming that the outside wall was perfectly insulated and that there was only radial variation in temperature. The bulk enthalpy at a section along the tube was calculated from a first law of thermodynamics heat balance, i. e., assuming that the increase in enthalpy between two sections is equal to the heat added to the flow between the sections. A computer program was written to reduce the data. A sample of the printout is shown in Fig. 19. The outlet temperature is calculated by a heat balance and compared with the measured temperature and the Nusselt number based on bulk properties at the relevant section is calculated. This is merely used as a reference for defining the heat transfer deterioration factor.

Figure 20 shows some representative  $T_{\text{wall}}$  versus Bulk Enthalpy curves for a heat flux of 50,000 BTU/ft.<sup>2</sup>-hr. It is seen that there is a sharp deterioration in heat transfer at higher heat fluxes. This takes place at a value of enthalpy that is substantially smaller than the critical enthalpy, the amount depending on the heat flux and flow rate. It has been

---

\* Near the critical region,  $dH/dT$  is very large and hence a small error in measuring the temperature can throw the enthalpy balance completely off. Heat balance checks in this region are thus relatively poor.

FIG.19 : DATA PRINT-OUT

PRESSURE 11cc,0	Q 47196,0000	G 1341145,00	TIN 74,0	TOUT 82,0	TCAL 89,8	TR 78,8	TWALL 156,8	H 604,9	ENTH 66,3	RATIO 2,20
						81,7	166,8	554,6	69,7	2,55
						83,3	155,8	650,7	72,0	2,27
						84,3	142,8	806,5	73,6	1,91
						85,5	137,8	902,1	75,3	1,81
						86,7	135,8	961,3	77,0	1,81
						87,5	132,8	1042,5	78,7	1,80
						88,3	127,8	1194,0	80,4	1,73
						89,0	127,8	1216,6	82,1	1,87
						89,1	127,8	1219,7	83,8	1,85
						89,2	125,8	1289,7	85,5	1,74
						89,3	125,8	1293,2	87,2	1,73
						89,4	122,8	1414,6	89,4	1,56

PRESSURE 11cc,0	Q 47196,0000	G 1690311,00	TIN 79,0	TOUT 84,0	TCAL 89,7	TR 81,9	TWALL 127,8	H 1027,2	ENTH 69,9	RATIO 2,07
						83,6	137,8	870,9	72,5	2,07
						84,7	133,8	961,2	74,3	1,96
						85,8	126,8	1150,6	75,7	1,74
						86,7	124,8	1238,3	77,0	1,69
						87,4	124,8	1260,8	78,3	1,76
						87,9	122,8	1354,2	79,7	1,74
						88,6	120,8	1463,7	81,0	1,77
						89,0	120,8	1485,2	82,4	1,84
						89,1	119,8	1537,4	83,7	1,77
						89,2	118,8	1593,4	85,0	1,70
						89,3	118,8	1597,6	86,4	1,69
						89,4	117,8	1659,7	88,2	1,61
						89,5	117,8	1669,0	90,8	1,59

U

U

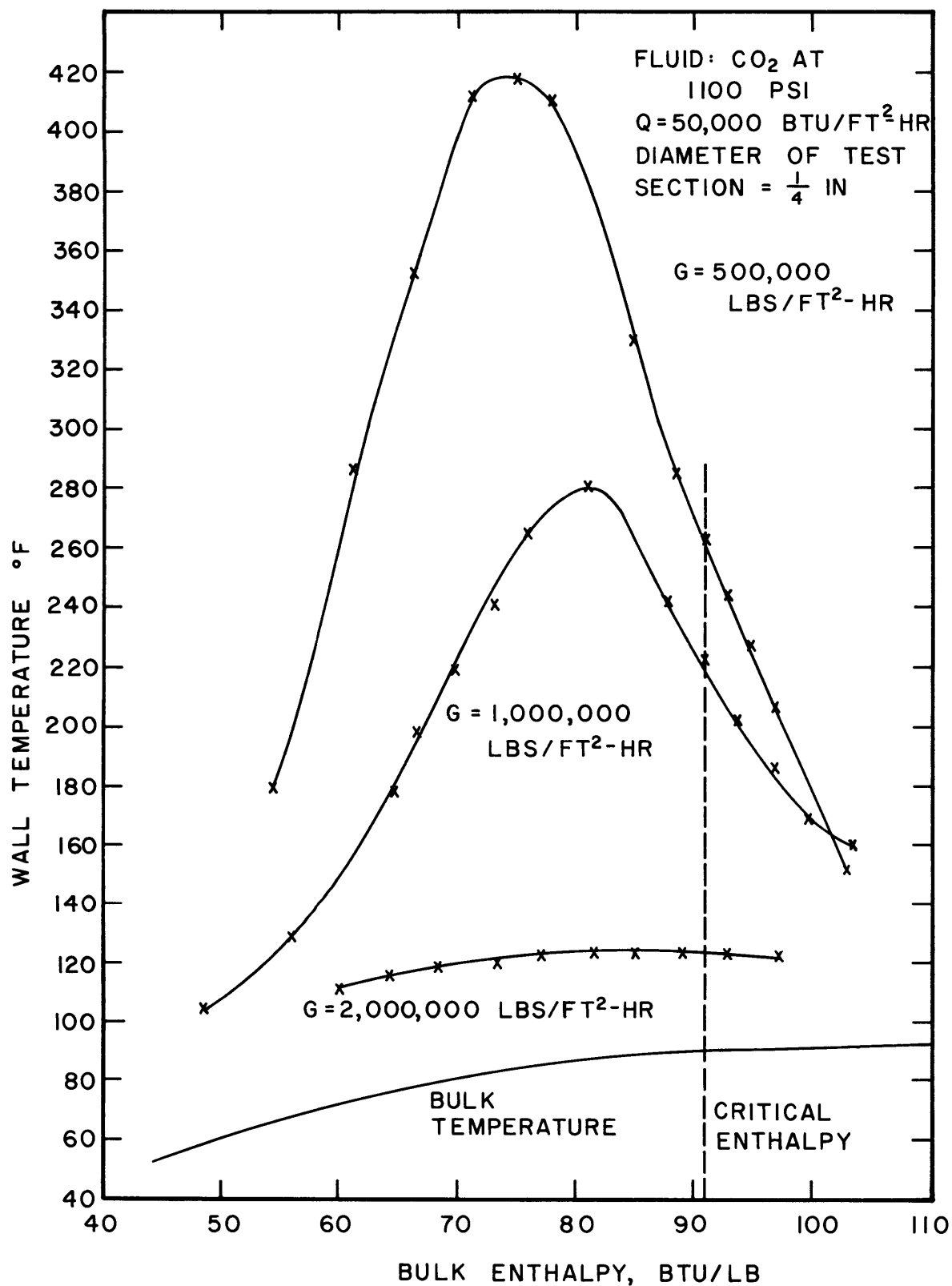


FIG. 20 EXPERIMENTAL RESULTS FOR CO<sub>2</sub> AT 1100 PSI

observed that the higher the ratio of heat flux to the flow rate, the worse is the deterioration and the earlier it occurs. It is thought that the chief reason this phenomenon has not been observed by earlier investigators is that they did not use low enough inlet temperatures, i. e., the results of Koppel and Smith (11), using an inlet temperature of 70°F appear to show the tail end of a temperature peak.

#### 5. Factors Affecting Deterioration

The amount and nature of the deterioration in heat transfer is sensitive to a number of factors.

1. The heat flux and flow rate. As mentioned earlier, the deterioration gets worse as the ratio of heat flux/flow rate is increased.
2. Inlet Enthalpy. The amount of deterioration is strongly influenced by the inlet enthalpy. It is worse when the inlet enthalpy is low. The effect of inlet enthalpy is shown in Fig. 21. When the fluid enters above a certain enthalpy, the deterioration is very small, even though the inlet enthalpy is below the critical enthalpy. This is tied in with the entrance effect which has considerable influence when the critical temperature is in the fluid film next to the wall in the entrance region. This effect would presumably be of little importance when the wall temperature in the entrance region is below the critical temperature.
3. Upstream conditions. Swirl, vibration or flow instabilities tend to reduce the amount of deterioration (Fig. 22). This is because of the tendency of such disturbances to disrupt the low density boundary layer near the wall. Tests are currently being performed with a test section with a swirl generating twisted tape in the entrance region, and preliminary experiments indicate that the deterioration is substantially reduced.

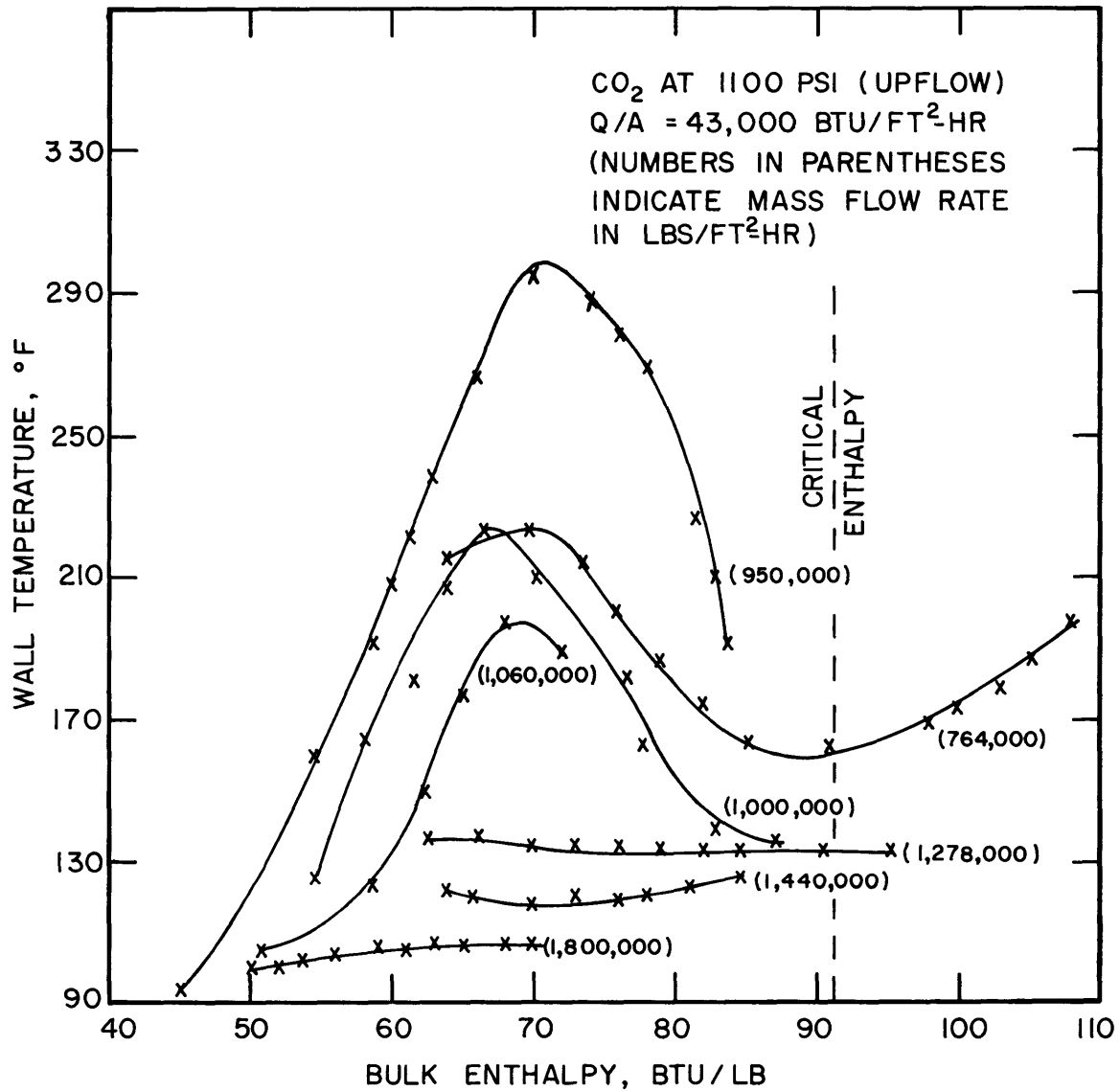


FIG. 21 : EXPERIMENTAL RESULTS SHOWING EFFECT  
 OF INLET ENTHALPY ON THE TEMPERATURE VS. LENGTH PROFILE

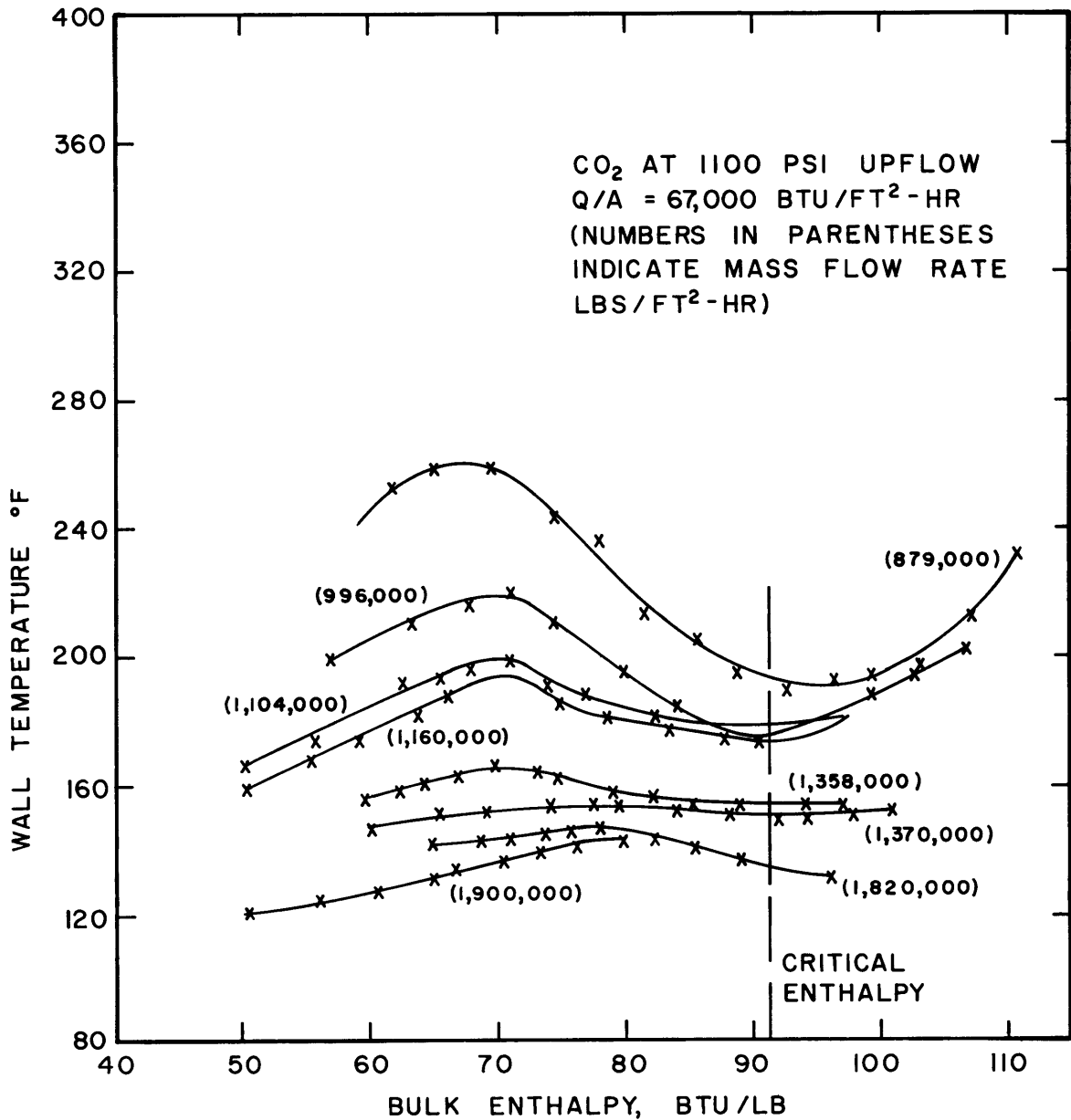


FIG. 22 EXPERIMENTAL RESULTS SHOWING EFFECT OF TUBE VIBRATION

4. Pressure. The deterioration is the worst when the system pressure is close to the critical pressure, where the changes in properties are the most rapid. Figure 23 shows some data taken at 1150 psi and a comparison of this data with comparable data at 100 psi shows that the hot spot at this pressure is lower and not as sharp as at the lower pressure. (See Fig. 26).
5. Scale Buildup. It is suspected that presence of scale on the heater surface aggravates the deterioration in heat transfer. No direct confirmation is available at present.
6. Orientation of the test section. Hot spots were obtained in both upflow and downflow. A more detailed comparison between the two is made in a later section.

#### 6. Comparison with Computed Wall Temperature Versus Bulk Enthalpy Curves

Due to the sensitiveness of the deterioration to upstream effects such as entrance effects and swirl, it is difficult to compare them representatively against the computed curves with the fully-developed profile assumptions. Most upstream effects, however, tend to reduce the deterioration in heat transfer so that at high heat fluxes the computed results should be expected to be in error on the high side. A comparison of calculated and experimental results is made in Fig. 24. The results compare in a manner similar to the steam results, i. e., the prediction of the hot spot is somewhat low at the inception of the experimental peak, but somewhat high at higher heat fluxes. Again, the prediction does not do a good job in the post-peak region.

#### 7. Experimental Safe Versus Unsafe Plot for CO<sub>2</sub>

A safe versus unsafe plot for carbon dioxide was constructed based on the same criterion as defined in Sec. 4.7, i. e., a run is unsafe if for

$$T_{\text{wall}} > T_{\text{crit}} > T_{\text{bulk}}$$

$$\frac{\text{Nu}_{\text{mac}}}{\text{Nu}} > 2.0$$

where

$$\text{Nu}_{\text{mac}} = 0.023 (\text{Re}_b)^{0.8} (\text{Pr}_b)^{0.4}$$

Nu = local Nusselt number

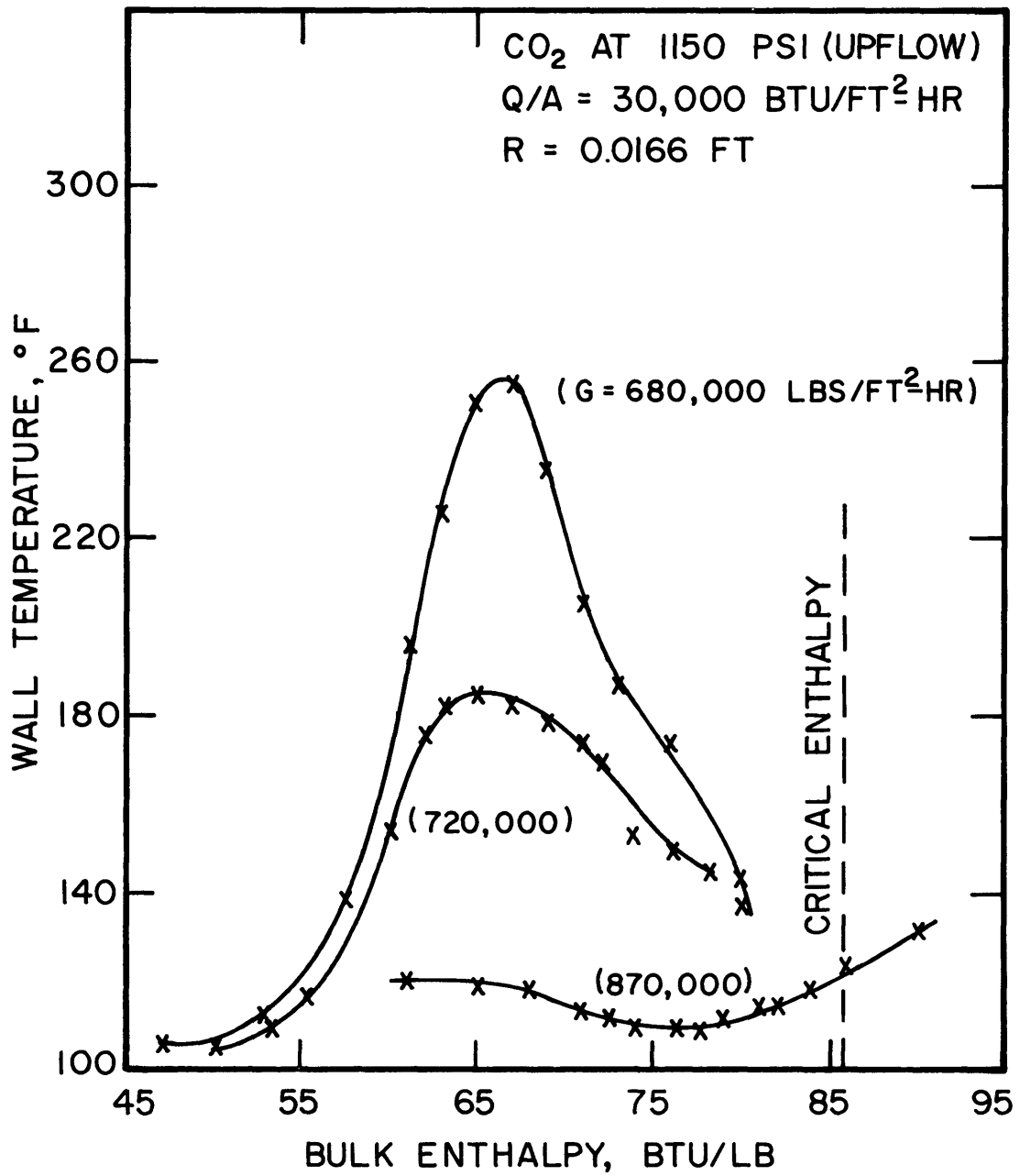


FIG. 23 : EXPERIMENTAL RESULTS FOR CO AT 1150 PSI

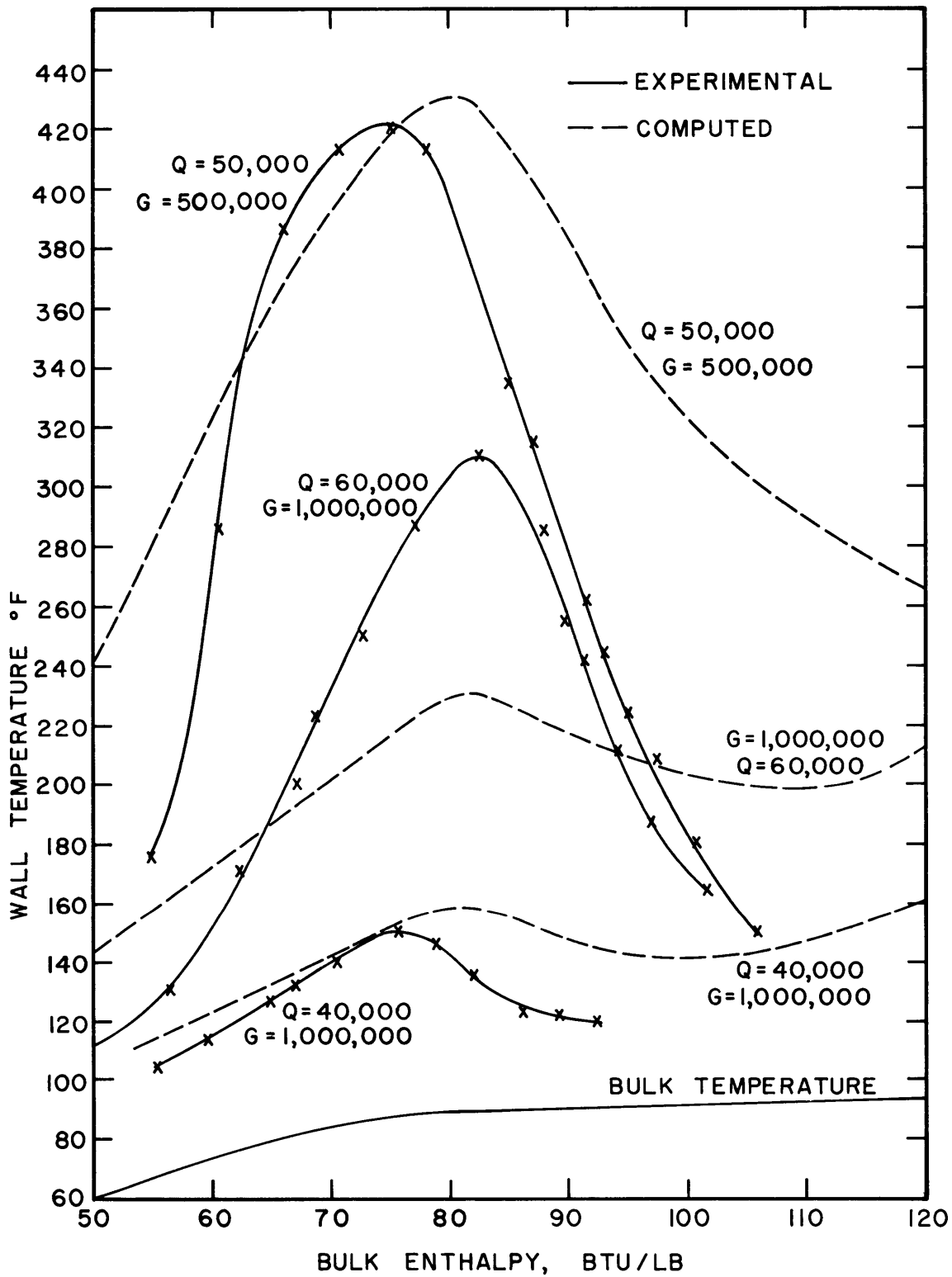


FIG. 24 COMPARISON BETWEEN COMPUTED AND EXPERIMENTAL WALL TEMPERATURE PROFILES FOR CO<sub>2</sub>

This plot for carbon dioxide at 1100 psi and upflow is shown in Fig. 25. A fairly clear demarcation can be made on this basis between safe and unsafe regions. Figure 26 shows the plot at 1150 psi and a comparison. With Fig. 25 is made to show that the deterioration in this case takes place at higher heat fluxes than at 1100 psi.

A corresponding plot was computed based on the properties of carbon dioxide at 1100 psi and the theoretical procedure outlined in Sec. 5.2. Figure 27 shows the plot obtained in this way. It is seen that the comparison between the computed and experimental limits is not as good in this case as with steam, at higher values of heat flux. This is probably due to the reason that enough sub-cooling was not available at the higher heat fluxes.

#### 8. Comparison Between Upflow and Downflow

In downflow, the free convection acts to decrease the heat transfer coefficient and a deterioration may be expected to take place at lower heat fluxes for corresponding flow rates. Some evidence to the contrary has been reported by Miropolskiy (8) working with water at very low flow rates and a larger diameter test section. However, with carbon dioxide, under the conditions tested, there was marked deterioration at high heat fluxes. Some representative runs are plotted in Fig. 28. Here, too, the effect of inlet enthalpy is important.

A safe versus unsafe plot for downflow is shown in Fig. 29. It appears that at large flow rates the deterioration takes place at lower heat fluxes than in upflow, but the situation reverses at small flow rates. More data at low flow rates is necessary before this trend can be confirmed.



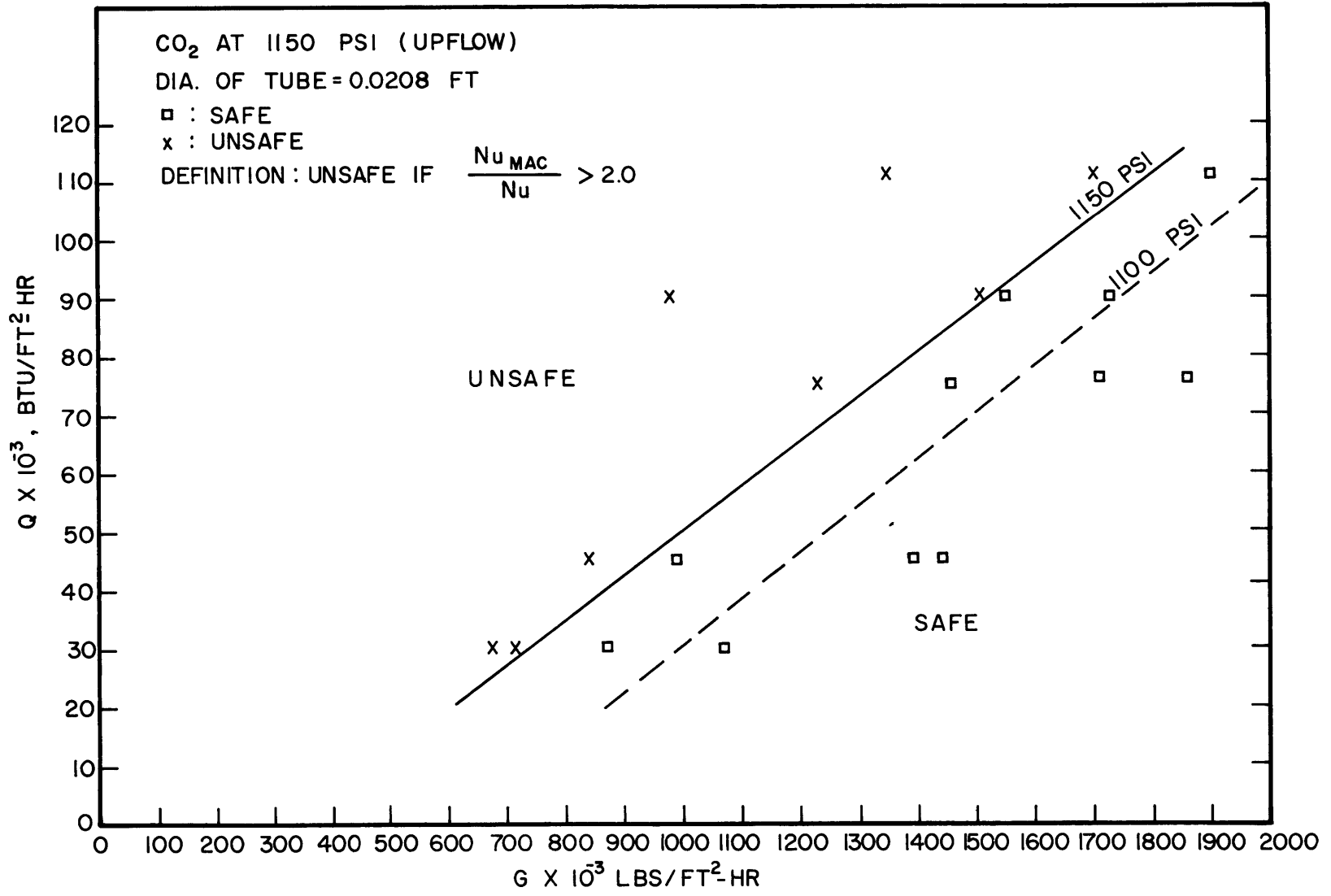


FIG. 26 : EXPERIMENTAL SAFE VS. UNSAFE PLOT FOR CO<sub>2</sub> AT 1150 PSI

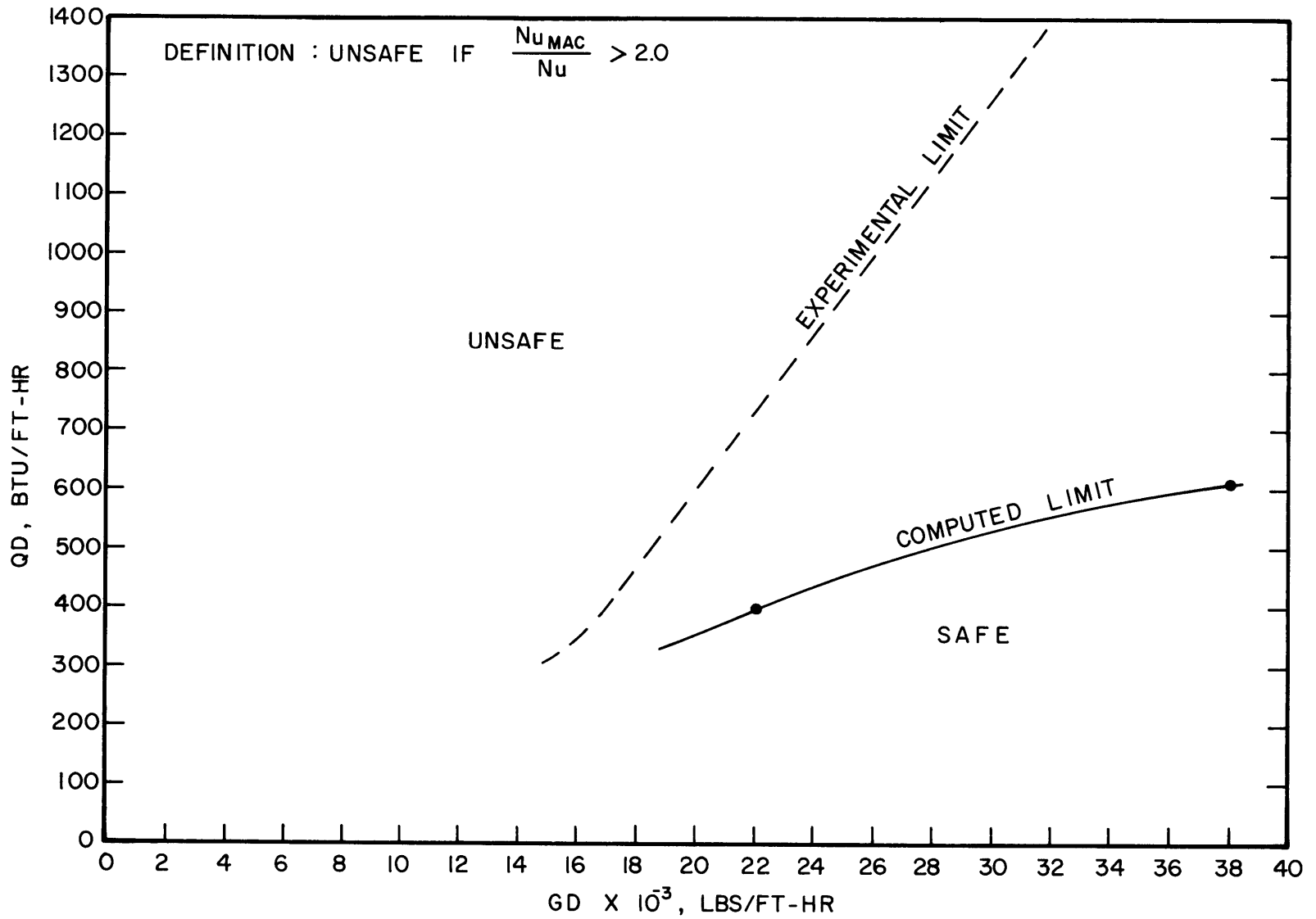


FIG. 27 : COMPARISON BETWEEN COMPUTED AND EXPERIMENTAL SAFE VS. UNSAFE PLOTS

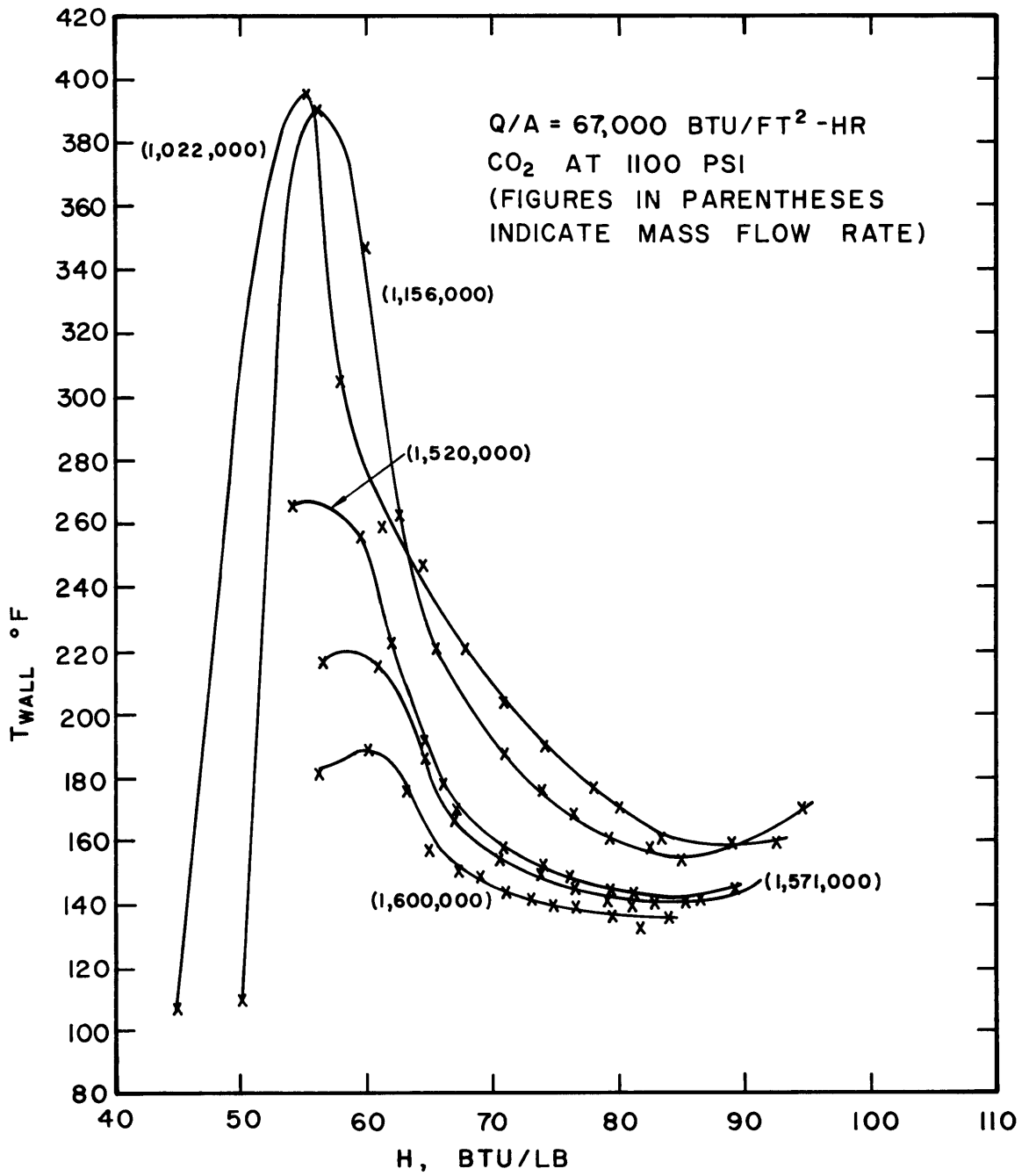


FIG. 28 EXPERIMENTAL RESULTS FOR DOWNFLOW

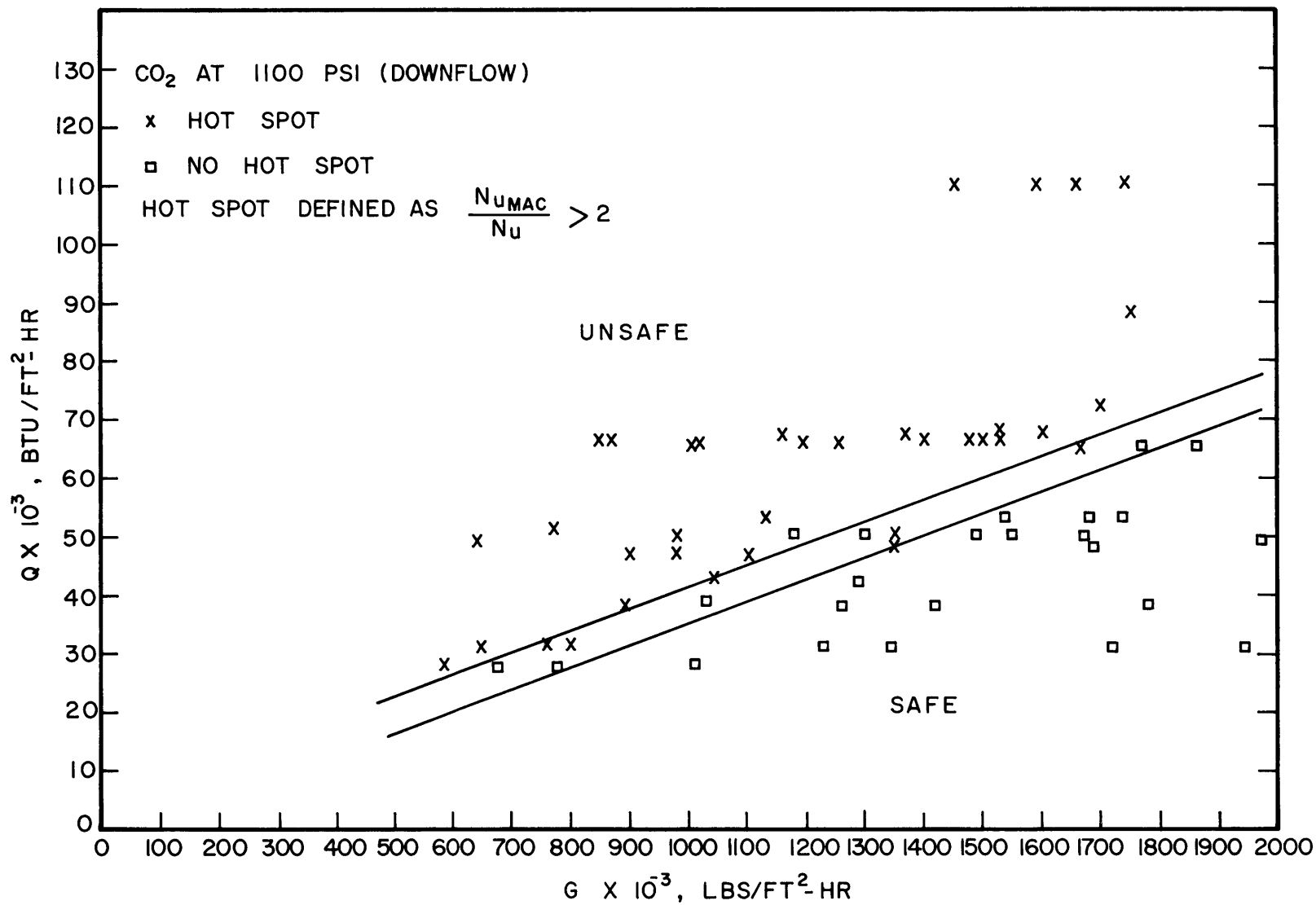


FIG. 29 EXPERIMENTAL SAFE VS. UNSAFE PLOT FOR DOWNFLOW

## 7. FUTURE WORK

It seems desirable that a visual study of the process be made, since carbon dioxide undergoes marked optical changes due to the drop in density and corresponding change in refractive index, in the critical region. For this purpose, it has been decided to use an annular test section with a stainless steel heater on the inside and gauge glass on the outside. Visual and photographic studies will be made.

In a recent study, Lopina (32) has shown that marked improvement in heat transfer can be obtained by using a twisted tape inside the test section to generate swirl, and has satisfactorily correlated the additional heat transfer to the convective effects of the swirl process. It is expected that introducing swirl would produce a large improvement in heat transfer in the supercritical region, because of the large differences in density. At present tests are being made with a small length of twisted tape inserted in the entrance region of the test section.

## 8. CONCLUSIONS

1. A region of deteriorated heat transfer can occur with high heat fluxes at supercritical pressure as long as the bulk temperature is below the psuedo-critical temperature. This occurs because the low density and thermal conductivity at the wall are not yet compensated by increased velocity in the core.
2. This deterioration can occur in either up or down flow.
3. The occurrence of the deteriorated region can be predicted reasonably well but the post deterioration behavior cannot because of inadequacies in the expressions used for eddy diffusivity.
4. The existence of the deterioration is sensitive to the details of the system geometry and the inlet subcooling.
5. Deteriorated heat transfer was never observed in CO<sub>2</sub> before because the inlet temperatures were not low enough in the other experiments.

## 9. REFERENCES

1. Shitsman, M.E., "Impairment of the Heat Transmission at Supercritical Pressures", *Teplofizika Vysokikh Temperatur*, Vol. I, No. 3, pp. 267 -275, 1963.
2. Vikrev, Yu V., and Lokshin, V.A., "An Experimental Study of Temperature Conditions in Horizontal Steam Generator Tubes at Supercritical Pressures", *Teploenergetika*, 11, pp. 79 - 82, 1964.
3. Miropolskiy, Z. L., Picus, V.J., and Shitsman, M.E., "Regimes of Deteriorated Heat Transfer at Forced Flow of Fluid in Curvilinear Channels", 3rd Annual Heat Transfer Conference, A.I.Ch.E., pp. 95 - 105, 1966.
4. Swenson, H.S., Carver, J.R., and Kakarala, C.R., "Heat Transfer to Supercritical Water in Smooth-Bore Tubes", *Jour. of Heat Transfer, Transactions ASME* 87, pp -477-483, 1965.
5. Powell, W.B., "Heat Transfer to Fluids in the Region of the Critical Temperature", *Jet Propulsion* 27, pp. 776-783, 1957.
6. Szetela, E.J., "Heat Transfer to Supercritical Hydrogen", *American Rocket Society Journal* 32, No. 8, pp. 1289 - 1292.
7. McCarthy, J.R., Seader, J.E., and Trebes, D.M., "Heat Transfer to Supercritical Nitrogen Tetroxide at High Heat Fluxes and in Axially Curved Flow Passages", *ASME Paper* 67-HT-69.
8. Miropolskiy, Z.L., Personal Communication with Prof. Griffith.
9. Hall, W.B., Jackson, J.D., and Khan, S.A. "An Investigation of Forced Convection Heat Transfer to Supercritical Pressure Carbon Dioxide", 3rd Annual Conference on Heat Transfer, I. Mech E. Section, pp. 257 - 266, 1966.
10. Bringer, R.P., and Smith, J.M., "Heat Transfer in the Critical Region", *A.I.Ch.E. Journal*, 3, pp. 49 -55 , 1957.

## 9. REFERENCES (Continued)

11. Koppel, L.B., and Smith, J.M., "Turbulent Heat Transfer in the Critical Region", International Developments in Heat Transfer, Part 3, ASME, pp. 579 - 585, 1961.
12. Tanaka, H., Nishiwaki, N., and Hirata, M., "Turbulent Heat Transfer to Supercritical Carbon Dioxide", Semi-International Symposium, J.S.M.E., Tokyo, September 1967.
13. Novak, E.S., Grosh, R.E., and Liley, P.E., "A Survey of P-V-T Data for Water in the Critical Region". Journ. of Heat Transfer, ASME 83 c, pp. 1 - 11, 1961.
14. Michels, A. Bijl, A., and Michels C., "Isotherms of CO<sub>2</sub>", Proc. Royal Society, London, A160, p. 376, 1937.
15. Michels, A., Blaise, B., and Michels, M., "Isotherms of CO<sub>2</sub> in the Neighborhood of the Critical Point and Round the Coexistence Line", Proc. Royal Society, London, A160, p. 358, 1937.
16. Michels, A., Botzen, A., and Schurmann, W., "The Viscosity of CO<sub>2</sub> Between 0 - 75°C and up to 200 Atmospheres", Physica 23, p. 95, 1957.
17. Michels, A., and Michels, M., "Isotherms of CO<sub>2</sub> Between 0 - 150°C and 1 - 250 Atmospheres", Proc. Royal Soc., London, A153, p. 201, 1935.
18. Michels, A., et al., "The Joule-Thomson Coefficient and the Specific Heat at Constant Pressure of CO<sub>2</sub>", Physica 14, p. 218, 1948.
19. Novak, E.S., and Grosh, R.J., "An Investigation of Certain Thermodynamic and Transport Properties of Water Vapor in the Critical Region", ANL-6064, October 1959.
20. Clark, A.L., "The Critical State of Pure Fluids", Chemical Review 23, p. 1, 1938.

## 9. REFERENCES (Continued)

21. Keesom, W.H., "Density of CO<sub>2</sub>", International Critical Tables, Vol. 3, p. 12, 1928.
22. Tzederberg, N.V., and Morosova, N.A., "Heat Conductivity of CO<sub>2</sub> at Pressures of 1 - 200 kg/cm<sup>2</sup> and Temperatures up to 1200°C", Teploenergetika 1, p. 75, 1960.
23. Hsu, Y.Y., and Smith, J.M., "The Effect of Density Variations on the Heat Transfer in the Critical Region", Trans. ASME 83, pp. 176 - 183, 1961.
24. Deissler, R.G., "Heat Transfer and Fluid Friction for Fully Developed Turbulent Flow of Air and Supercritical Water with Variable Fluid Properties", Trans. ASME 76, pp. 73 - 85, 1954.
25. Rohsenow, W.M., and Choi, H.Y., "Heat, Mass and Momentum Transfer", Prentice-Hall Pub. Co., p. 190.
26. Deissler, R.G., "Analytical and Experimental Investigation of Adiabatic Turbulent Flow in Smooth Tubes", NACA TN-2138, 1950.
27. van Driest, E.R., "On Turbulent Flow Near a Wall," Jour. Aeronaut. Sci., 23, p. 1007, 1956.
28. Spalding, D.B., "A Single Formula for the 'Law of the Wall'", Jour. App. Mech., 28, E, p. 455, 1961.
29. Sleicher, C.A., Jr., "Turbulent Flow of Newtonian Systems", Modern Chemical Engineering, Vol. I, Physical Operations, Reinhold Pub. Corp., pp. 45 - 89.
30. Goldmann, K., "Heat Transfer to Supercritical Water and Other Fluids with Temperature Dependent Properties", Chem. Engr., Prog. Symposium Series, Nuclear Engr., Part I, Vol. 50, No. 11, 1954.
31. Knapp, K.K., and Sabersky, R.H., "Free Convection Heat Transfer to Carbon Dioxide near the Critical Point", International Journal of Heat and Mass Transfer, Vol. 19, pp. 41 - 51, 1966.

## 9. REFERENCES (Continued)

32. Lopina, R.F., and Bergles, A.E., "Heat Transfer and Pressure Drop in Tape Generated Swirl Flow", Thesis (ScD.), Dept. of Mech. Engr., Mass. Inst. of Tech., 1967.
33. Styrikovich, M.A., Margulova, T.Kh., and Miropolskiy, Z.L., "Problems in the Development of Designs of Supercritical Boilers", Teploenergetika, 14(6), pp. 4 - 7, 1967.